Journal of Achievements in Materials and Manufacturing Engineering
VOLUME 31
ISSUE 2
December
2008

# Multilayer and gradient PVD coatings on the sintered tool materials

**L.A. Dobrzański*, K. Gołombek, J. Mikuła, D. Pakuła**
Division of Materials Processing Technology, Management and Computer Techniques in Materials Science, Institute of Engineering Materials and Biomaterials, Silesian University of Technology, ul. Konarskiego 18a, 44-100 Gliwice, Poland
* Corresponding author: E-mail address: leszek.dobrzanski@polsl.pl

Received 15.09.2008; published in revised form 01.12.2008

**Manufacturing and processing**

## ABSTRACT

**Purpose:** The paper presents investigation results of structure and properties of the multilayer and gradient TiN+(Ti,Al,Si)N+TiN nanocrystalline coatings deposited with the PVD method (CAE -Cathodic Arc Evaporation process) and in the combination of $Al_2O_3$ and TiN coatings in the CVD process on the substrate of cemented carbides, cermets, $Al_2O_3$+$ZrO_2$, $Al_2O_3$+TiC, $Al_2O_3$+$SiC_{(w)}$ oxide ceramics and $Si_3N_4$ nitride ceramics.
**Design/methodology/approach:** The structural investigation includes the metallographic analysis on the transmission and scanning electron microscope, confocal microscope. Examinations of the chemical compositions of the deposited coatings were carried out using the X-ray energy dispersive spectrograph EDS, glow-discharge optical emission spectroscope GDOS, and using the X-ray diffractometer. The investigation includes also analysis of the mechanical and functional properties of the material: substrate hardness tests and microhardness tests of the deposited coatings, surface roughness tests, evaluation of the adhesion of the deposited coatings, cutting properties of the investigated materials.
**Findings:** Deposition of the multicomponent gradient coatings with the PVD method, based on the Al and Si solid secondary solution in the TiN titanium nitride, isomorphous with the alternating pure titanium nitride TiN, on tools made from oxide, nitride ceramics and tool cermets, results in the increase of mechanical properties in comparison with uncoated tool materials, deciding thus the improvement of their working properties.
**Practical implications:** Deposition of (Ti,Al,Si)N nanocrystalline coatings by the use of PVD method causes the increase of cutting properties of tools made of cermets for ca. 300% and of $Al_2O_3$+$ZrO_2$ for ca. 100% comparing to adequately uncoated tools.
**Originality/value:** Comparison of the wide range of modern sintered tool materials with wide unique set of PVD coatings.
**Keywords:** Cutting tools; Cemented carbides; Cermets; Oxide and nitride ceramics; Surface layer; PVD

## 1. Introduction

The goal of the contemporary of machining technology is the constant increase of durability of the highly efficient cutting tools made with the powder metallurgy method enabling machining at high cutting speed. Fast pace of development of engineering and manufacturing technology brings the necessity for increasing the requirements posed to the contemporary sintered tool materials as regards their working properties, mechanical properties and abrasion wear resistance. Functional properties of many products and their elements depend not only on their capability to carry the mechanical loads by the element's entire cross-section from the material used or on its physical and chemical properties, but very often or mostly on its structure and properties of its surface layers. Economical considerations also dictate using the ennobling technologies for surface layer, which ensure the required service properties, making it possible to use simultaneously the possibly

inexpensive materials for the element's core, from which lower service properties are usually required. The contemporary technologies of materials forming employed in the machining, plastic forming, casting, and also plastics forming domains call for using more and more efficient tool materials. These requirements pertain mostly to the extension of life and reliability of tools used in machining processes, and also of limiting employment of cutting fluids still commonly used, however degrading the environment considerably. Improvement of the functional properties of tools and reduction of the ecological threats may be accomplished by employing the technology of putting down hard coatings on tools in the CVD or PVD processes, mostly by improvement of the tribological contact conditions in the cutting zone and by eliminating the cutting fluids. Deposition of hard wear resistant coatings feature one of the fastest developing directions of research, stimulated by the growing service requirements of machines and equipment, making definite improvement of the sintered tool materials possible (sintered high speed steels, cemented carbides, cermets, ceramics). The dynamic development in this area refers to new coating deposition methods, using better and better materials for coatings, constituting hard layers, and – first of all - optimising their functional properties. Compound coatings, whose structure and properties may be in addition optimised by solution reinforcement offer the best chances for fulfilling these expectations.

The paper presents the study of selected results of researches carried out by the authors and described in detail in works [1-21]. The goal of this paper is to compare the structure and properties of the PVD and CVD coatings deposited on sintered tool materials. Tools covered with coatings based on carbides, borides, nitrides, and oxides can work at higher service parameters (temperature and load). Moreover, the multilayer and multicomponent coatings developed relatively not so long ago make it possible to constitute freely properties of the entire coating as well as of its transition layer, ensuring good adhesion, compensation of the internal stresses, and transmission of the external loads. Tools with such coatings reveal a significant service life extension compared to the uncoated tools or coated with simple coatings based on mononitrides or carbonitrides, improvement of the tribological contact conditions in the tool-chip-machined material contact zone, and protection of the tool edge from oxidation and extensive overheating. Many aspects pertaining to forming of coatings, including also the process conditions effect on their properties, still remain inexplicable in spite of the enormous interest paid in them by many industrial centres and research laboratories. Moreover, each combination of the substrate material – coating type – deposition method calls for determining properties of the coated material and defining, based on them, the range of its possible applications. Research in this area is concentrated among other on searching the new composite gradient coatings, both multicomponent and multilayer ones, and adding new elements to coating combinations used since many years, like silicon or vanadium to TiAlN. Therefore, sintered tool materials were investigated in this paper, coated with the PVD method with the composite multilayer III generation gradient coatings of the TiN+ gradient(Ti,Al,Si)N+TiN and TiN + multi(Ti,Al,Si)N + TiN, and they were compared with the commercially available uncoated tool materials and those coated in the PVD and CVD processes with the single- and multilayer wear resistant coatings [1-50].

## 2. Materials and experimental procedure

The investigations were carried out on the multi-point inserts made from the cemented carbides, cermets, $Al_2O_3$+$ZrO_2$, $Al_2O_3$+TiC and $Al_2O_3$+$SiC_{(w)}$ oxide ceramics and $Si_3N_4$ nitride ceramics uncoated and coated using the PVD method in the CAE process, with the TiN+gradient (Ti,Al,Si)N+TiN and TiN+multi(Ti,Al,Si)N+TiN wear resistant coatings and combination of $Al_2O_3$ and TiN coatings in the CVD process. Specifications and chemical composition of the investigated materials are presented in Table 1. The parameters used in coating deposition are presented in earlier works [1-20].

Evaluation of the phase composition of the investigated coatings and substrates was made using the DRON 2.0 X-ray diffractometer, using the filtered cobalt lamp rays with the voltage of 40 kV and heater current of 20 mA.

The diffraction examinations and examinations of thin foils were made on the JEOL 3010CX transmission electron microscope (TEM) at the accelerating voltage of 300 kV. The diffraction patterns from the transmission electron microscope were solved using the computer program. Thin foils were made in the longitudinal and transverse sections from the 0.2-0.5 mm thick laminae cut from the solid specimens, from which 3 mm O.D. disks were cut out, with the initially ground and levelled surfaces. The lamellae were next mechanically thinned on the Disc Grinder to thickness of about 80 μm and ion polished using the Gatan firm equipment.

The metallographic examinations of the investigated materials were made on the Philips XL-30 and OPTON DSM940 scanning electron microscopes. To obtain the fracture images the SE and BSE detection methods were used with the accelerating voltage in the range of 15-20 kV.

Topography examinations of the tool surface after scratch test were carried out on the OLYMPUS LEXT OLS3000 confocal microscope.

In case of coatings deposited on nitride ceramic substrates the measurements of textures and phase composition were made with the Seifert-FPM XRD 7 X-ray diffractometer. The X-ray radiation was used of the Co Kα cobalt lamp with the 35 kV supply voltage and current of 40 mA. Analysis of the investigated coatings texture was made using the inverse pole figures method. Intensity of the (111), (002), (022) and (113) diffraction lines was analysed – in case of the TiC, TiN and Ti(C,N) phases, and of the (012), (104), (110), (113), (116), (030), and (1010) ones in case of the $Al_2O_3$ phase. The line intensity was measured after the graphical separation of the overlaying lines and after isolating the clear profile of the analysed line. The measured line intensity was divided by the relative intensity of this line specified in the catalogues, and in case of the Ti(C,N) phase diffraction lines – by the value interpolated using the TiC and TiN catalogue values. Basing on these values and on location of traces normal to the (001), (011), (111) and (113) planes – the equal density isolines of spatial distribution of the normal direction to the sputtered plane (KN) were plotted in the base triangle. Further, the figures were normalized to make determining the isolines values possible in units being multiples of density for the uniform distribution in the space that is for the specimen that does not reveal texture. This made it possible to assess how strongly the investigated specimens are textured.

Table 1.
Chemical composition of the investigated materials

| Designa-tion | Type | Producer | Coating | | | Process type | Roughness, μm |
|---|---|---|---|---|---|---|---|
| | | | Type | Composition | Thickness, μm | | |
| 890 | cemented carbides | Seco | uncoated | | | | 0.36 |
| A30N | cemented carbides | Sumitomo | | | | | 0.35 |
| CM | cermet | Seco | | | | | 0.22 |
| T130A | cermet | Sumitomo | | | | | 0.20 |
| WidialoxG | $Al_2O_3$+$ZrO_2$ | Widia | | | | | 0.21 |
| CC 650 | $Al_2O_3$+TiC | Sandvik | | | | | 0.07 |
| CC 670 | $Al_2O_3$+$SiC_{(w)}$ | Sandvik | | | | | 0.26 |
| NS260 | $Si_3N_4$ | Sumitomo | | | | | 0.06 |
| 890 | cemented carbides | Seco | gradient layer | TiN+ (Ti,Al,Si)N+TiN | 4.0 | PVD | 0.65 |
| A30N | cemented carbides | Sumitomo | | | 4.0 | | 0.64 |
| CM | cermet | Seco | | | 4.0 | | 0.60 |
| T130A | cermet | Sumitomo | | | 4.0 | | 0.62 |
| WidialoxG | $Al_2O_3$+$ZrO_2$ | Widia | | | 2.0 | | 0.43 |
| CC 650 | $Al_2O_3$+TiC | Sandvik | | | 1.8 | | 0.37 |
| CC 670 | $Al_2O_3$+$SiC_{(w)}$ | Sandvik | | | 2.5 | | 0.37 |
| NS260 | $Si_3N_4$ | Sumitomo | | | 2.0 | | 0.45 |
| 890 | cemented carbides | Seco | multi layer | TiN+multi (Ti,Al,Si)N+TiN | 4.0 | | 0.67 |
| A30N | cemented carbides | Sumitomo | | | 4.0 | | 0.66 |
| CM | cermet | Seco | | | 4.0 | | 0.62 |
| T130A | cermet | Sumitomo | | | 4.0 | | 0.63 |
| WidialoxG | $Al_2O_3$+$ZrO_2$ | Widia | | | 2.3 | | 0.37 |
| CC 650 | $Al_2O_3$+TiC | Sandvik | | | 1.5 | | 0.27 |
| CC 670 | $Al_2O_3$+$SiC_{(w)}$ | Sandvik | | | 2.8 | | 0.33 |
| NS260 | $Si_3N_4$ | Sumitomo | | | 4.0 | | 0.40 |
| T130Z | cermet | Sumitomo | | TiN+TiC+TiN | 5.0 | | 0.79 |
| NS260 | $Si_3N_4$ | Sumitomo | two layer | TiN+$Al_2O_3$ | 10.0 | CVD | 0.45 |
| WidialoxG | $Al_2O_3$+$ZrO_2$ | Widia | | | 6.0 | | 0.40 |
| CC 650 | $Al_2O_3$+TiC | Sandvik | | | 5.8 | | 0.29 |
| CC 670 | $Al_2O_3$+$SiC_{(w)}$ | Sandvik | | | 7.9 | | 0.30 |
| IS80 | $Si_3N_4$ | Iscar | | $Al_2O_3$+TiN | 2.6 | | 0.25 |

In case of coatings deposited on oxide ceramic and cermet substrates the measurements of textures and phase composition were made with the diffractometric Schulz X-ray reflection method on the Bruker D8 Advance diffractometer equipped with Euler disk. The X-ray cobalt anode lamp was used, providing the radiation of the 1.79Å wavelength. Because of the employed X-ray reflection method, changes of the inclination of the normal to the specimen in respect to the goniometer axis were from 20 to 90 degrees. Inclination angles were changed every 5 degrees. Pole figures obtained in this way include the following angle ranges: for α from 0˚ to 360˚, and for φ from 0˚ to 70˚. Three pole figures were measured for each specimen: for {111}, {200}, and {220} planes. Orientation distribution functions were calculated from the figures. The Burker software included in the diffractometer service pack was used for calculations. Full pole figures were calculated for {111}, {200}, and {220} planes from the orientation distribution function.

Changes of the chemical concentrations of the coating constituents in the direction perpendicular to its surface and of concentrations in the interlayer between the coating and the substrate material were evaluated basing on examinations made in the LECO Instruments glow-discharge optical emission spectroscope GDOS-850A. The following spectrometer Grimm lamp working conditions were set during the examinations: lamp internal diameter – 4 mm; lamp power supply voltage – 700 V; lamp current – 20 mA; working pressure – 100 Pa. The continuous concurrent spectrometer in the Paschen-Runge configuration was used in the device, with the focal length of 750 mm, with the holographic mesh of 2400 lines per millimeter. The maximum depth of the chemical composition analysis is a dozen or so μm.

The $R_a$ roughness parameter of the uncoated and coated surfaces was determined on the RankTaylor Hobson Surftec 3+ device with the measurement length of 0.25 mm. The measurements were made in two orthogonal directions with the measurement accuracy of 0.01 μm.

The microhardness tests of coatings were made on the SHIMADZU DUH 202 ultra microhardness tester. Test conditions were selected so that the required and comparable test results would be obtained for all analyzed coatings. Measurements were made at 0.07 N load, eliminating influence of the substrate on the measurement results.

Adhesion evaluation of the coatings on the investigated inserts was made using the scratch test on the CSEM REVETEST device, by moving the diamond penetrator along the examined specimen's surface with the gradually increasing load. The tests were made with the following parameters: load range 0-200 N, load increase rate (dL/dt) 100 N/min, penetrator's travel speed (dx/dt) 10 mm/min, acoustic emission detector's sensitivity AE 1. The critical load $L_C$, at which coatings' adhesion is lost, was determined basing on the registered values of the acoustic emission AE and friction coefficient $F_t$. Additionally $L_c$ was determined optically.

The working properties of the developed coatings were determined basing on the technological cutting tests carried out at room temperature. Cutting ability of the investigated materials was determined basing on the technological continuous cutting tests of the EN-GJL-250 grey cast iron and C45E steel. The VB = 0.20 (oxide ceramics, cermets) and 0.30 mm (nitride ceramics) width of the wear band on the surface of the tool used for machining was the criterion of the cutting edge consumption evaluation. The following parameters were used in the machining capability experiments: feed rate f = 0.10; 0.15; 0.20 mm/rev; depth of cut $a_p$ = 1; 2 mm; cutting speed $v_c$ = 200; 400m/min.

## 3. Discussion of the experimental results

### 3.1. Structure of substrates

Basing on the examinations of thin foils in the transmission electron microscope it was found out that the structure of the investigated cemented carbides is the $\gamma$solid solution of cobalt with dispersed carbides, mostly of the WC type. Structure of the thin foil from the cemented carbide of the A30N type is presented in Figure 1. Moreover, it was found out that the average diameter of the significant portion of tungsten carbide particles is smaller than 0.5 μm, which clearly classifies the investigated carbide as belonging to the fine-grained materials group. Based on the examinations of thin foils from the cermet substrate it was found out that the structure consists of the $\gamma$solid solution of cobalt and nickel, filling the hard skeleton formed mostly from the Ti(C,N) particles. Structure of the thin foil from the T130A type cermet is presented in Figure 2. In case of the Ti(C,N) particles it was found out that their sizes are in the range from 0.5 μm to 1.0 μm. Crystalline structure defects were observed also in the characteristic shell-core structure. Basing on the examinations of thin foils parallel to the coating surface in the transmission electron microscope it was found out that the $Al_2O_3$+$ZrO_2$ oxide tool ceramics contains the aluminium oxide grains with the hexagonal lattice and the $ZrO_2$ ones with the monoclinic lattice occurring in the twinned lamellae form (Fig. 3) in case of the $Al_2O_3$+TiC oxide tool ceramics contains the aluminium oxide grains with the hexagonal lattice and the TiC ones with the hexagonal lattice (Fig. 4).

Based on the examinations of thin foils in the transmission electron microscope it was found out that the structure of the investigated $Si_3N_4$ nitride tool ceramics (NS260) is the β-$Si_3N_4$ phase. Moreover, it was found out that the size of the significant portion of the β-$Si_3N_4$ phase particles is smaller than 500 nm, which unequivocally classifies the investigated ceramics to the fine-grained materials (Fig. 5).

a)

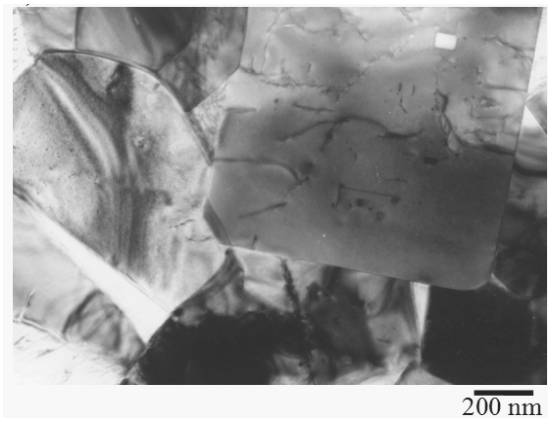


b)

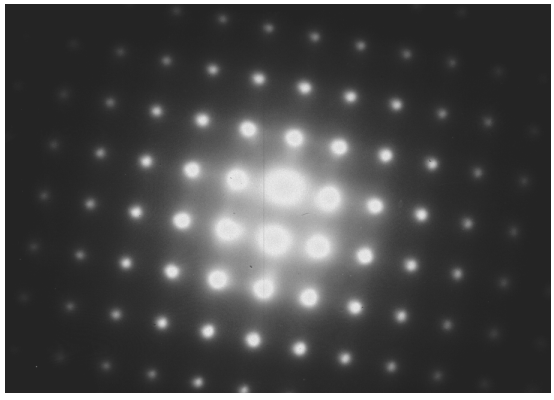

c)

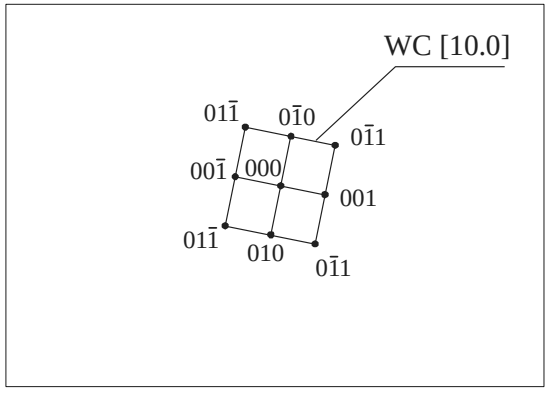


Fig. 1. Structure of 890 type cemented carbides substrate (TEM): a) bright field, b) diffraction pattern from the area as in figure a, c) solution of the diffraction patterns from figure b

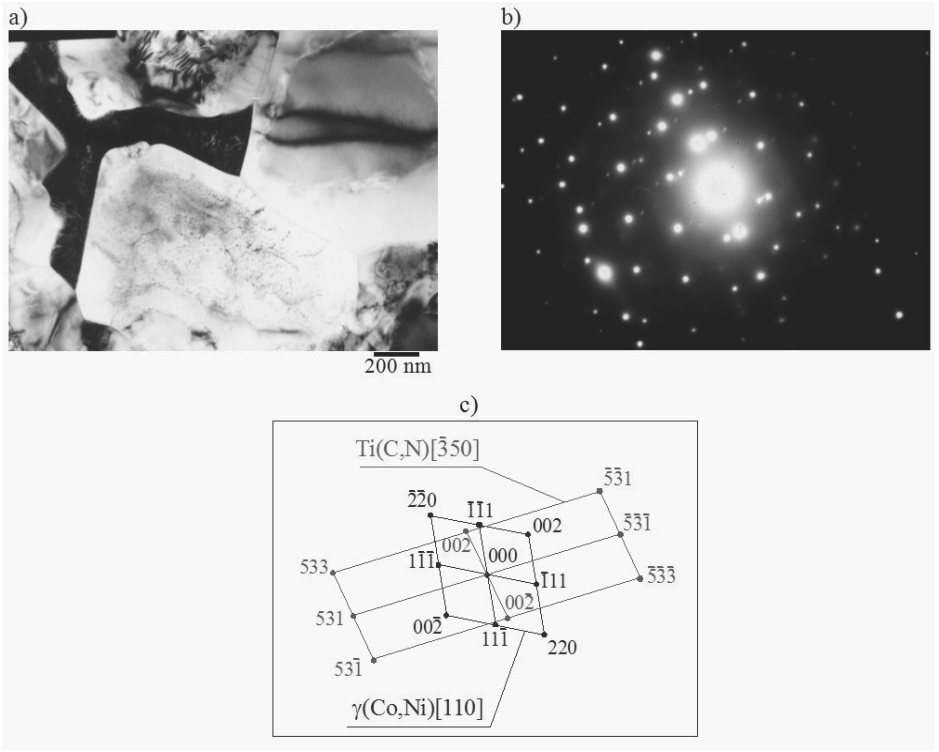


Fig. 2. Structure of T130A type cermet substrate: thin foil structure parallel to the layer surface (TEM): a) bright field, b) diffraction pattern from the area as in figure a, c) solution of the diffraction patterns from figure b

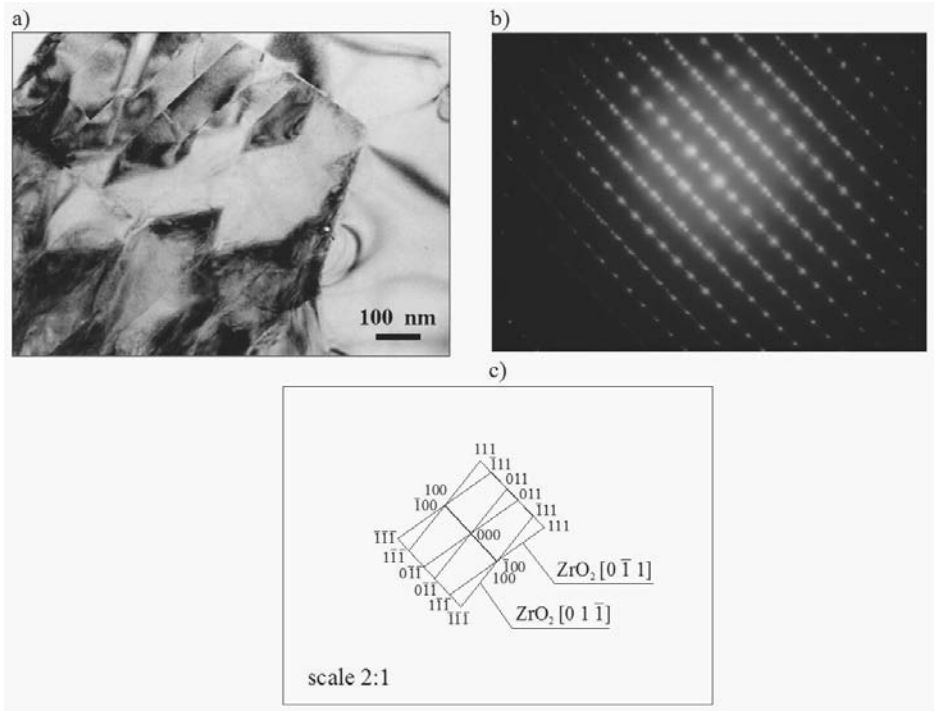


Fig. 3. Structure of $Al_2O_3$+$ZrO_2$ substrate: thin foil structure parallel to the layer surface (TEM): a) bright field, b) diffraction pattern from the area as in figure a, c) solution of the diffraction patterns from figure b (2:1 scale)

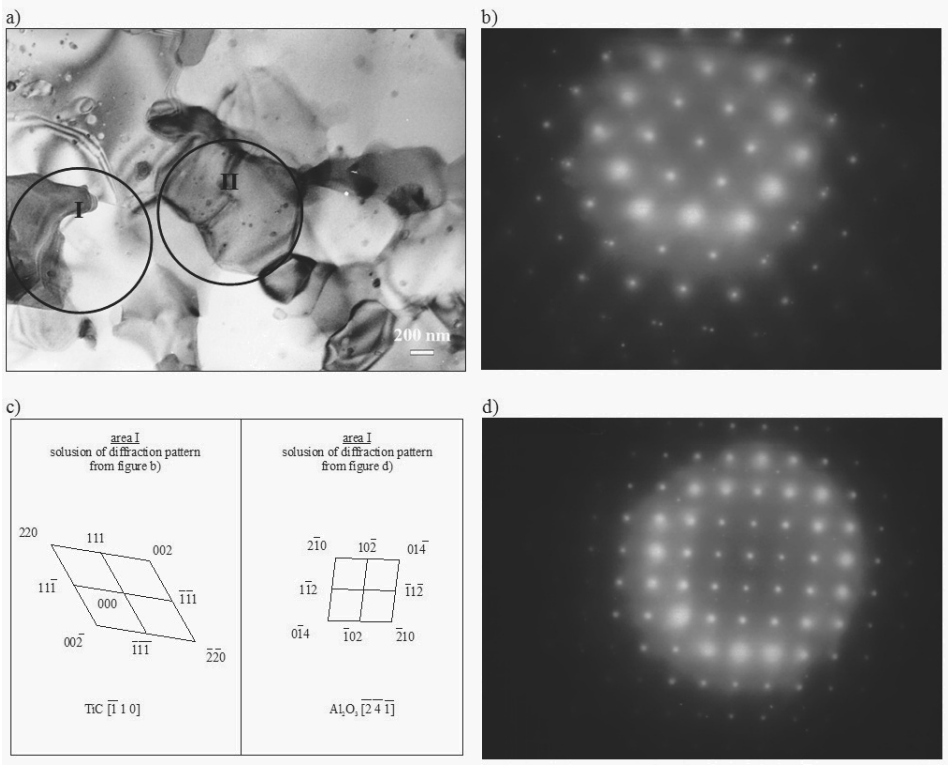


Fig. 4. Structure of $Al_2O_3$+TiC substrate: thin foil structure parallel to the layer surface (TEM): a) bright field, b) diffraction pattern from the area I as in figure a, c) solution of the diffraction patterns from figures b,d, d) diffraction pattern from the area II as in figure a.

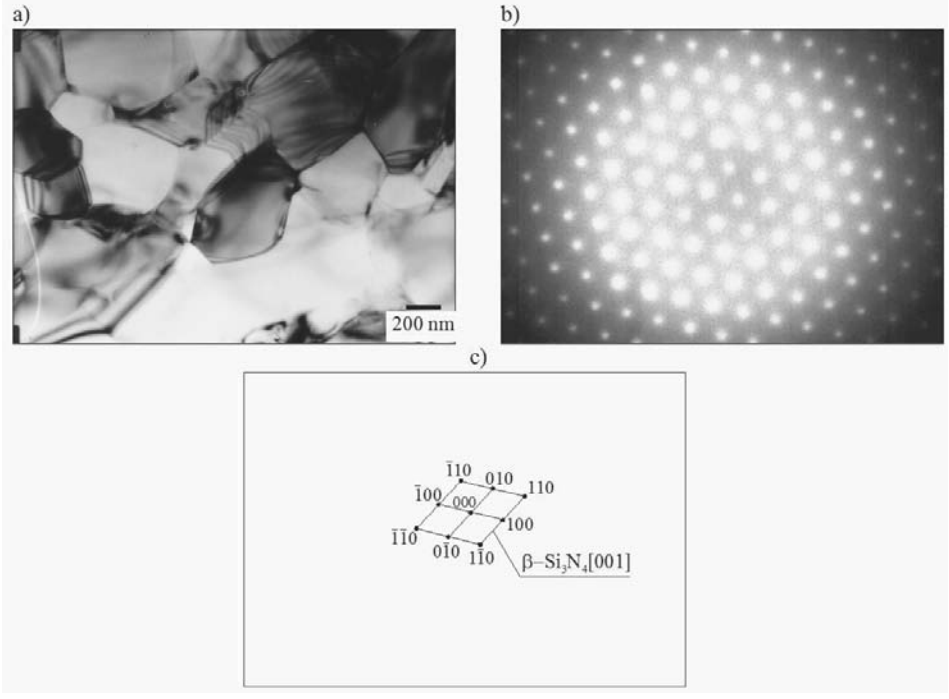


Fig. 5. Structure of tool nitride ceramics $Si_3N_4$ (NS260); thin foil structure parallel to the layer surface (TEM): a) bright field, b) diffraction pattern from the area as in figure a, c) solution of the diffraction pattern from figure b

## 3.2. Structure of deposited coatings

Examinations of thin foils from coatings confirm that, according to the original assumptions, coatings containing the TiN type phases were deposited onto the cemented carbides and cermets substrates. It is not feasible to differentiate these phases from the diffraction point of view, due to isomorphism of the TiN and (Ti,Al,Si)N phases. Structure of coatings deposited onto the cemented carbides presented in Figures 6 and 7.

a)

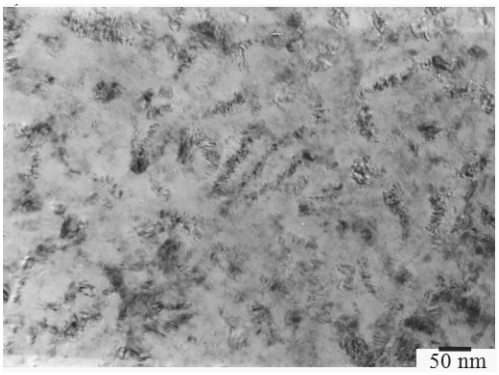


b)

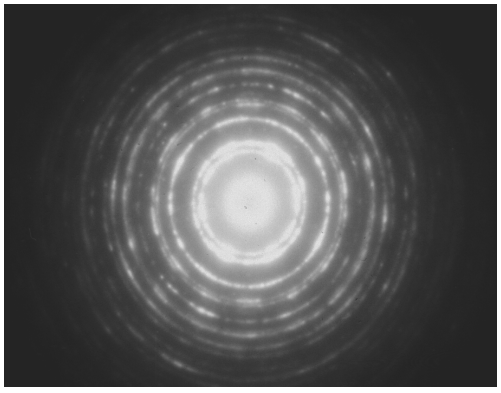

c)

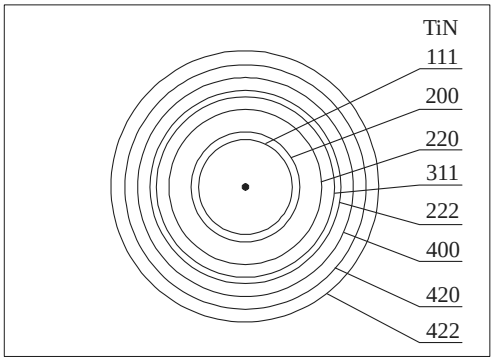


Fig. 6. a) Structure of the thin foil from the TiN+multi(Ti,Al,Si)N+TiN coating deposited onto the 890 type cemented carbide, b) diffraction pattern for the area as from figure a, c) solution of the diffraction pattern from figure b.

a)

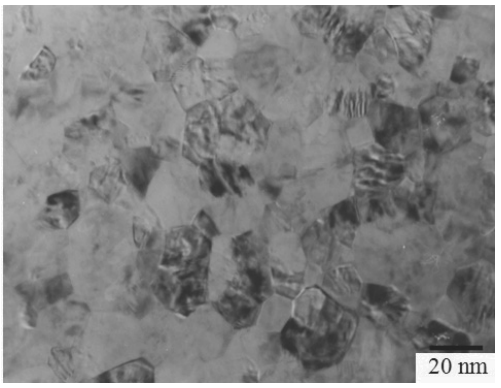


b)

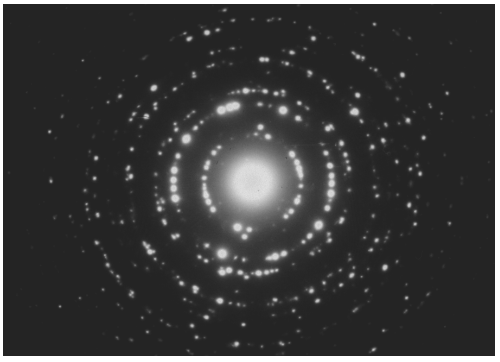

c)

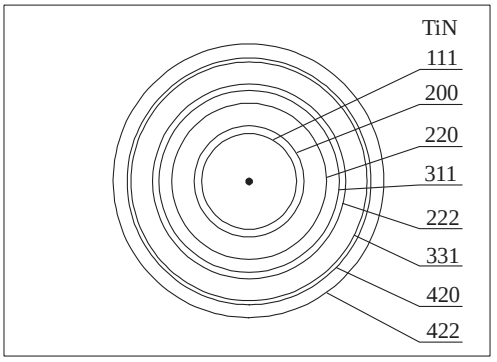


Fig. 7. a) Structure of the thin foil from the TiN+multi(Ti,Al,Si)N +TiN coating deposited onto theT130A type cermet, b) diffraction pattern from the area as in figure a, c) solution of the diffraction pattern from figure b.

It was found out that the TiN+TiAlSiN+TiN coating deposited onto the $Al_2O_3$+$ZrO_2$ substrate is characteristic of the columnar structure of the TiN layer (Fig. 8), confirmed by texture examinations and in case of the other layers, even at the largest magnifications used, no grain boundaries were revealed, which may attest to their fine-grained structure which was confirmed by thin foils examinations on the transmission electron microscope (Fig. 9).

a)

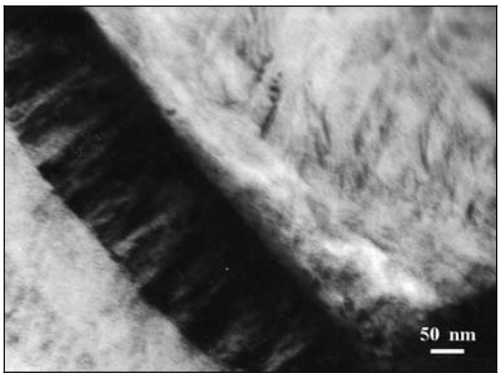


b)

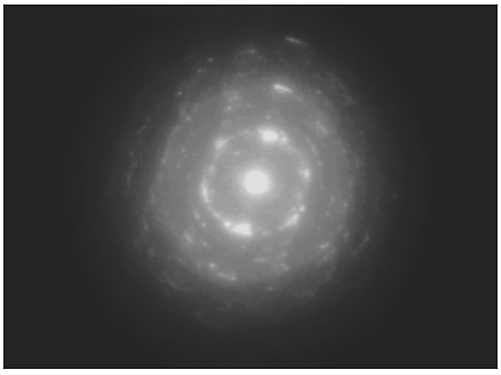

c)

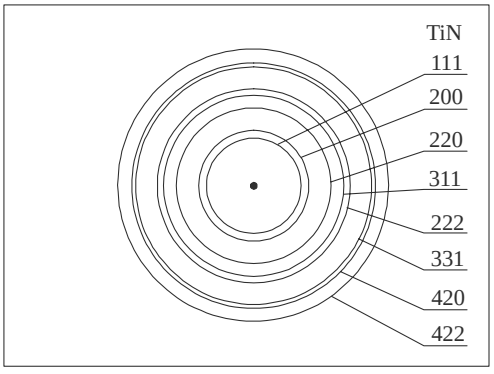


Fig. 8. Structure of TiAlSiN layer deposited on $Al_2O_3$+$ZrO_2$ substrate: thin foil structure parallel to the layer surface (TEM): a) bright field, b) diffraction pattern from the area as in figure a, c) solution of the diffraction patterns from figure b.

a)

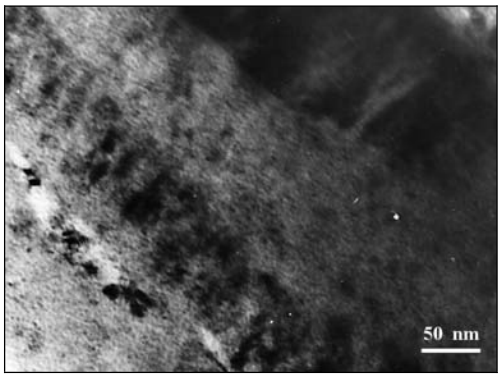


b)

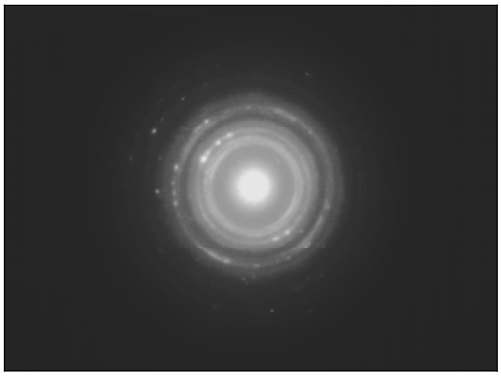

c)

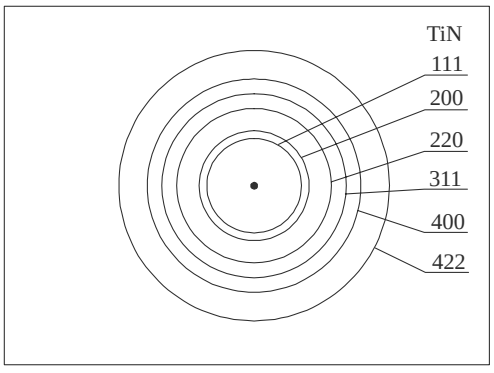


Fig. 9. Structure of TiAlSiN layer deposited on $Al_2O_3$+$ZrO_2$ substrate: thin foil structure parallel to the layer surface (TEM): a) bright field, b) diffraction pattern from the area as in figure a, c) solution of the diffraction patterns from figure b.

Examinations of thin foils from the TiN+$Al_2O_3$ (CVD) coating confirm that, according to the original assumptions, coatings containing the TiN and $Al_2O_3$ type phases were deposited onto the nitride tool ceramics substrate. The observed TiN structure in the thin foil, parallel to the surface of the investigated coating, is characteristic of fine grains, which is confirmed, among others, by reflex rings in the diffraction patterns coming from the fine-crystalline phases. Examination results of the thin foil from the transverse section of the TiN+$Al_2O_3$ coating indicate that the TiN coating has a columnar structure; whereas, the $Al_2O_3$ layer – the coarse-grained structure. There is an interface between the TiN and $Al_2O_3$ layers, where the fine grains of these phases are found. Occurrences of the scarce fine-grained $Al_2O_3$ grains with the monoclinic structure were revealed in this zone, unlike the typical structure of the $Al_2O_3$ phase with the trigonal lattice, which occurs outside of this border area over the entire layer width (Figs. 10, 11).

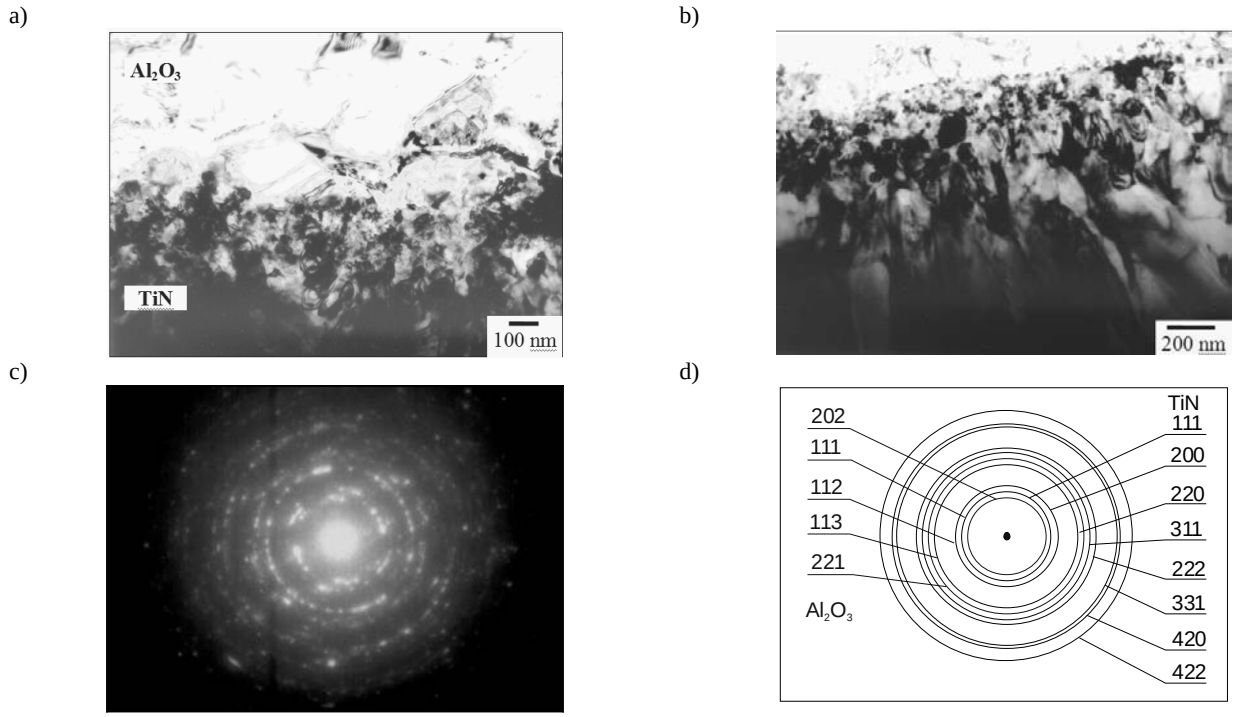


Fig. 10. a) Structure of TiN+$Al_2O_3$ coating: thin foil from cross section of the layer surface (TEM): b) bright field, c) diffraction pattern from the area as in figure b, d) solution of the diffraction pattern from figure c

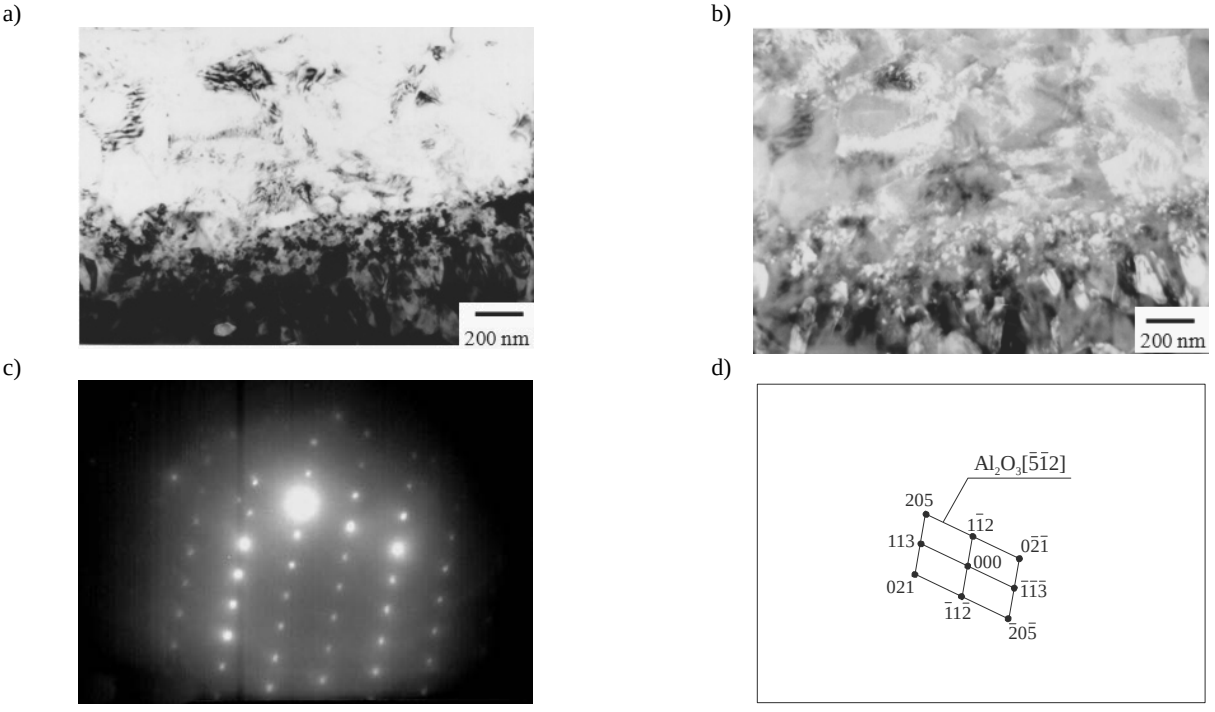


Fig. 11. a) Structure of TiN+$Al_2O_3$ coating: thin foil from cross section of the layer surface (TEM): b) dark field, c) diffraction pattern from the area as in figure a, d) solution of the diffraction pattern from figure c

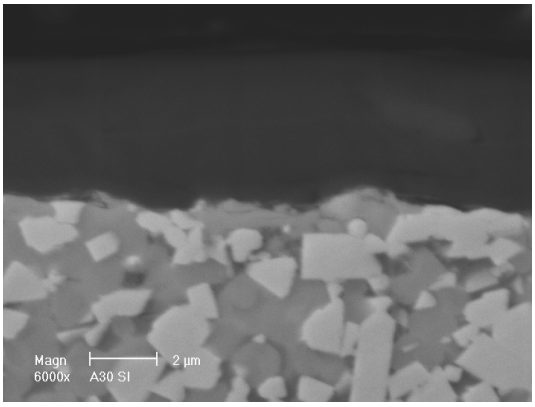


Fig. 12. Fracture surface of the TiN+(Ti,Al,Si)N +TiN gradient coating deposited onto the A30N type cemented carbide substrate

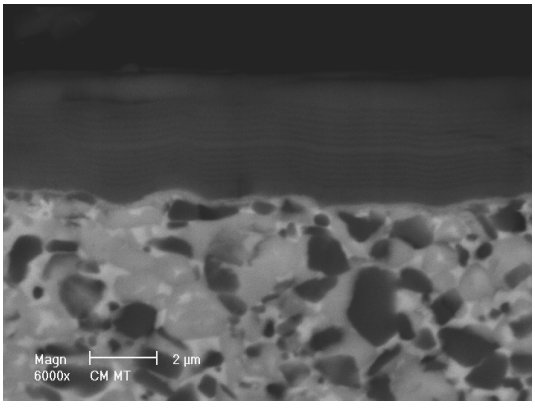


Fig. 13. Fracture surface of the TiN+multi (Ti,Al,Si)N+TiN coating deposited onto the CM type cermet substrate

The fractographic examinations carried out that give grounds to state that the coatings were deposited uniformly onto the investigated substrate materials and that they are characteristic of the depending on the coating type employed, and that the particular layers adhere tightly to themselves and to the substrate (Fig. 12-15, 20). Examinations of the chemical compositions of the coatings carried out using the X-ray energy dispersive spectrograph EDS confirm presence of the relevant elements in the deposited coatings and their layers (Fig. 14b-14d, 20b).

Topography observations of the investigated PVD coatings reveal their inhomogeneity connected with occurrences of multiple drop shaped micro-particles on coating surface, which is connected with the nature of the employed coating deposition PVD process character – Cathodic Arc Evaporation. This effect is undoubtedly connected with difference of the thermal conductivity coefficients of the nitride coating and pure titanium droplets, and difference of stresses between the coating and these micro-particles, developing during cooling of the substrate surface after completing the coating deposition process. Therefore, the

a)

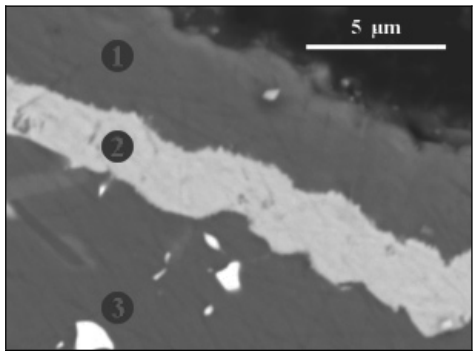


b)

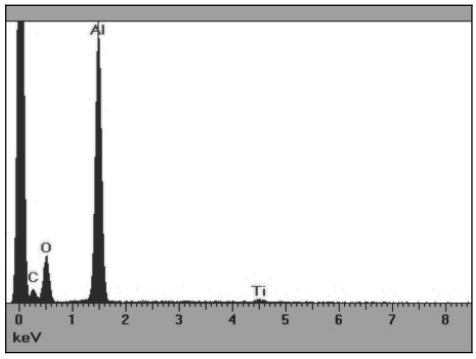


c)

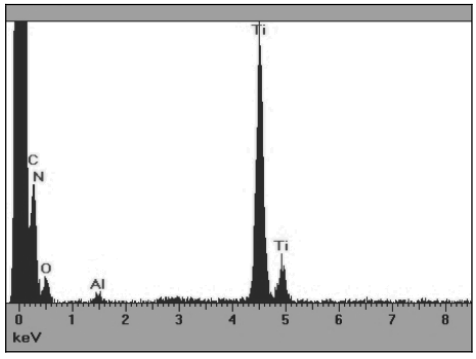


d)

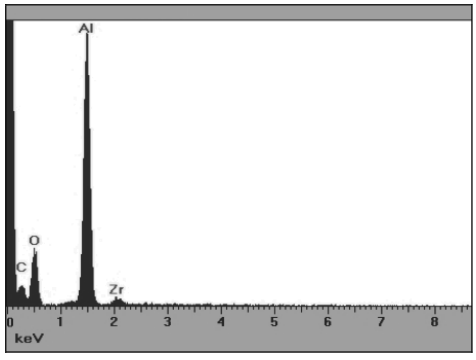


Fig. 14. a) Fracture surface of the TiN+$Al_2O_3$ coating deposited on $Al_2O_3$+$ZrO_2$ substrate, b) X-ray energy dispersive plot the area 1 as in figure a, c) X-ray energy dispersive plot the area 2 as in figure a, d) X-ray energy dispersive plot the area 3 as in figure a.

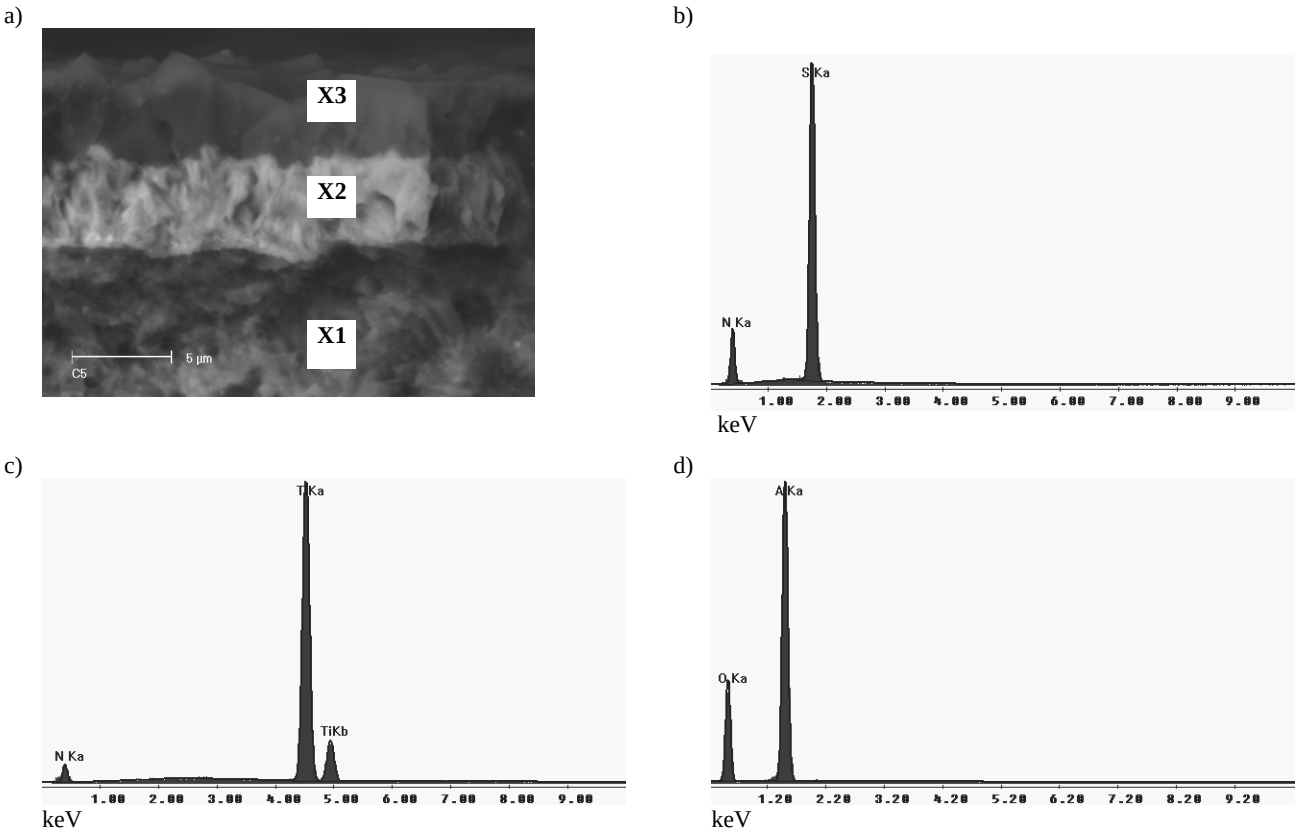


Fig. 15. a) Fracture surface of the TiN+$Al_2O_3$ coating deposited on $Si_3N_4$ substrate, b) X-ray energy dispersive plot the area 1 as in figure a, c) X-ray energy dispersive plot the area 2 as in figure a, d) X-ray energy dispersive plot the area 3 as in figure a

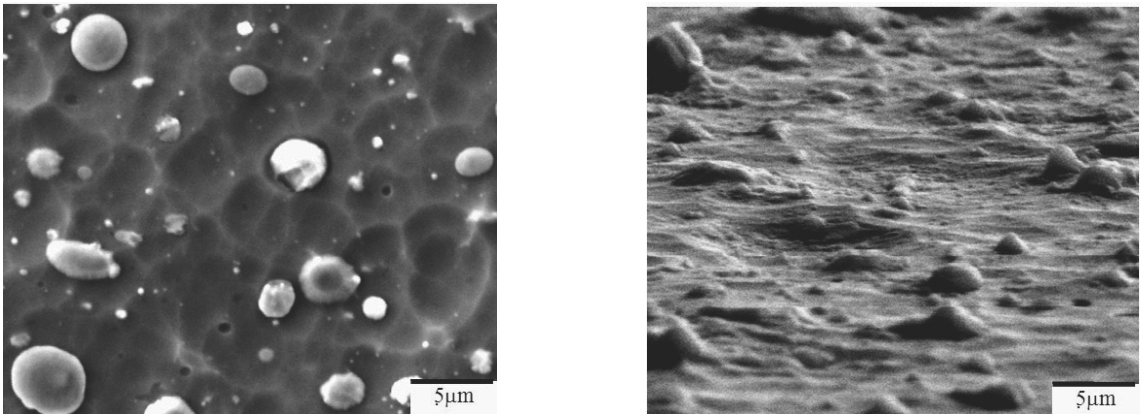


Fig. 16. Topography of the TiN+multi (Ti,Al,Si)N+TiN coatings surface, deposited on the 8 type cemented carbide substrate

surfaces of coatings demonstrate inhomogeneities connected with occurrences of the droplet shaped and elongated micro-particles, originating probably by their spattering when they hit the substrate surface during coating deposition process (Figs. 16, 24a). Sizes of these micro-particles are differentiated and vary from several tenths of a micrometer to more than 10 µm, whereas in case of the elongated particles their size exceeds even 15 µm. Examinations of the chemical compositions of the droplet shaped micro-particles made using the X-ray energy dispersive spectrometer (EDS) indicate that titanium dominates inside of these micro-particles, which suggests that they are the pure titanium droplets knocked out from the titanium disk, which settle

and solidify on the substrate surface (Figs. 17, 24b,d, Table 2). These droplets can settle on an already partially developed coating, and the coating can also develop on surface of the solidified titanium droplet, which was confirmed by the chemical composition analysis of the micro-particle surfaces, carried out using the EDS method.The black CVD coating completed with $Al_2O_3$ has another surface topography. The surface of TiN+$Al_2O_3$ coating is characteristic of significant inhomogeneity, roughness with the sharp upturned particles (Fig. 18b).

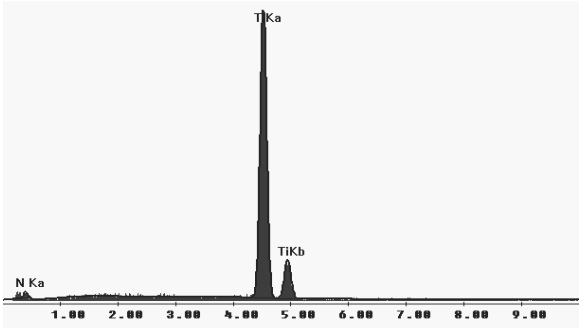


Fig. 17. Plot of the X-ray dispersive energy spectrometer measurement from the droplet surface developed on the TiN+multi (Ti,Al,Si)N+TiN on 890 cemented carbides

Table 2
Quantitative analysis of the chemical composition of droplet developed on the TiN+TiAlSiN+TiN coating deposited onto the 890 type cemented carbide

| Element | Mass concentration of the element [%] | Atomic concentration of the element [%] |
|---|---|---|
| N | 1.32 | 4.61 |
| Ti | 98.68 | 95.39 |
| Total | 100.00 | 100.00 |

It was demonstrated, using the X-ray qualitative phase analysis methods, that – according to the initial assumptions – coatings containing the TiN type phases, and most probably the complex (Ti,Al,Si)N nitride one, were developed on surfaces of the investigated materials (Fig. 19, 21c). Differentiation of the TiN and (Ti,Al,Si)N phases using the diffraction methods is impossible due to their isomorphous nature, as (Ti,Al,Si)N is – in fact – the secondary solid solution based on titanium nitride TiN. Moreover, reflexes occurring from the cemented carbide and $Al_2O_3$+TiC oxide ceramics substrates were found in the X-ray diffraction patterns, coming probably from the macro-particles deposited onto the coating surface (Figs. 19, 21c).

Occurrence of the prevailing axial texture with the privileged {100} coating growth plane was revealed basing on texture examination, parallel to the coating surface with the variable texturing. In case when the particular phase was put down in several layers, one should assume that the presented pole figures have a nature of the averaged values, and the pole figure shape of the particular phase is mainly influenced by the outer layer. In case of the coatings deposited onto the oxide tool ceramics occurrence of the {100}+{110}double texture was found; however, in all cases the {100} component dominates and the {110} one is clearly weaker.

a)

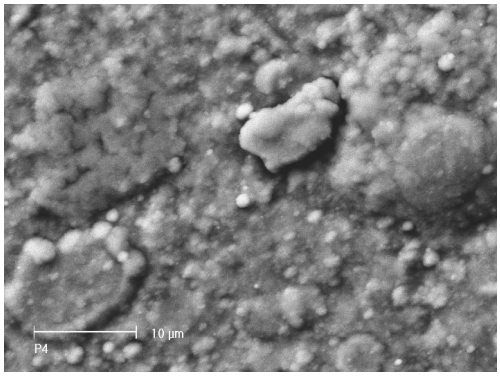


b)

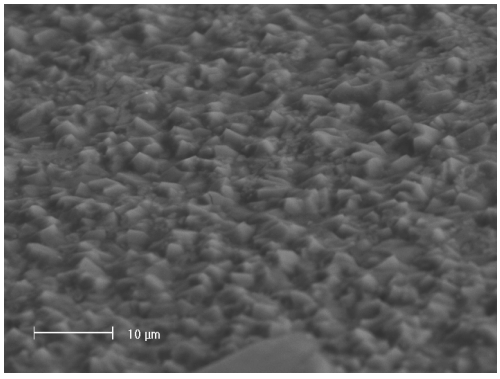


Fig. 18 a) Topography of the TiN+TiAlSiN+AlSiTiN and b) TiN+$Al_2O_3$ coatings surface deposited onto the $Si_3N_4$ nitride ceramics substrate

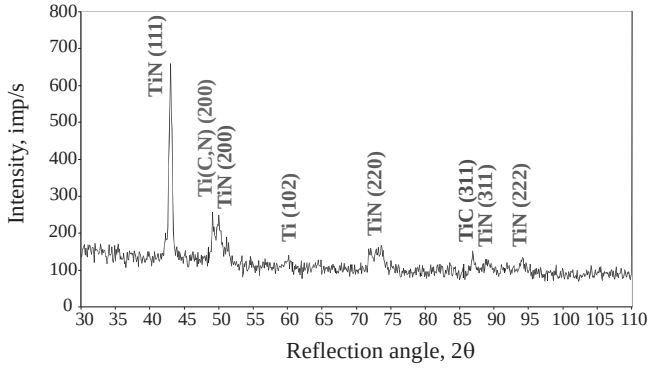


Fig. 19. X-ray diffractions pattern of the cermets with the TiN+(Ti,Al,Si)N+TiN gradient coating

a) b)

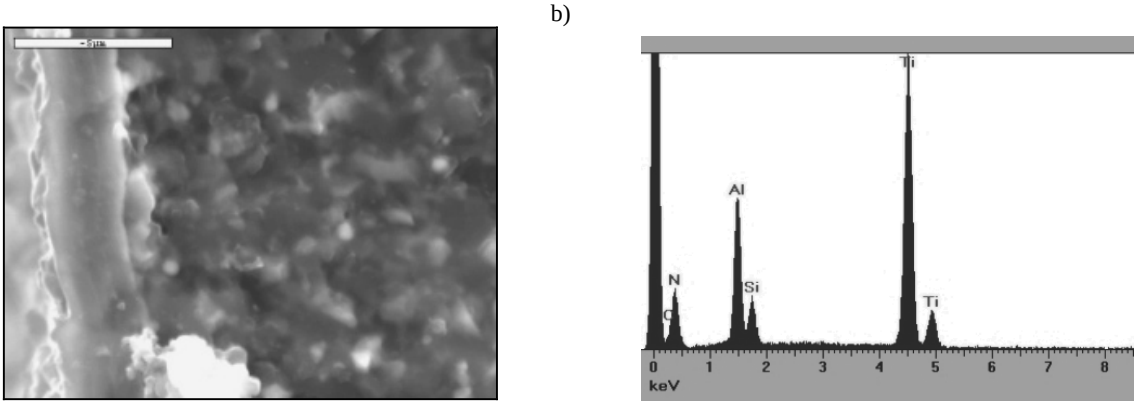


Fig. 20. a) Fracture surface, b) X-ray energy dispersive plot of the TiN+multiTiAlSiN+TiN coating deposited on $Al_2O_3$+TiC substrate

a) b)

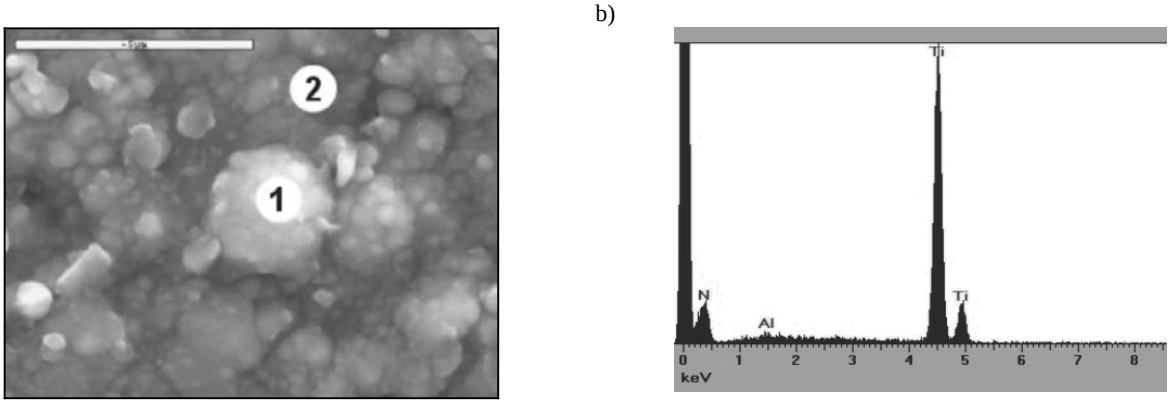


c) d)

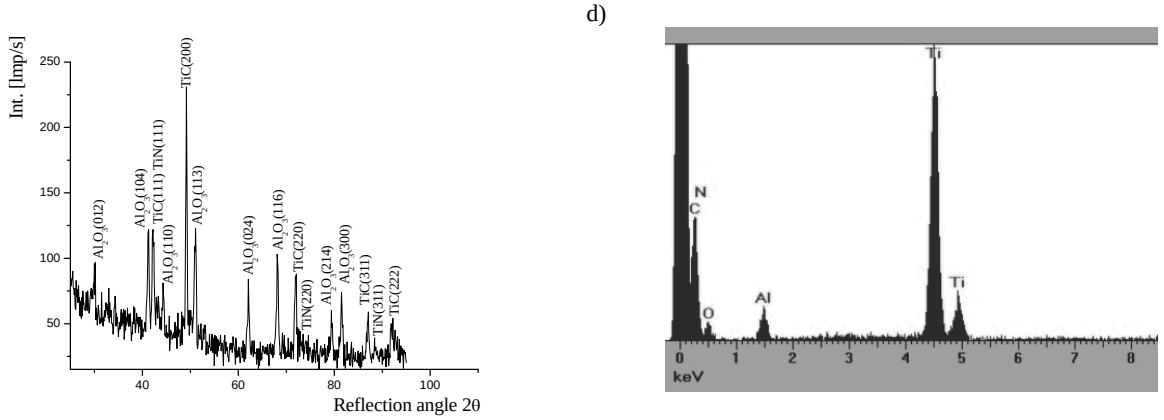


Fig. 21. a) Topography of the TiN+TiAlSiN+TiN coating surface, deposited on the $Al_2O_3$+TiC oxide ceramics, b) X-ray energy dispersive plot from the area 1 as in figure a, c) X-ray phase analysis, d) X-ray energy dispersive plot from the area 2 as in figure a

In case of texture of the investigated coatings on the nitride ceramics, when the particular phase was deposited in several layers, the presented pole figures should be treated as the averaged figures for all layers of that phase; however, bearing in mind that it is not an arithmetic average: the outer layer has the biggest effect on the pole figure of the particular phase. This is not that important, assuming that textures of all layers are similar. Most of the pole figures prove that the texture of the TiN layers deposited is very weak. It is especially weak in the specimens with the TiN+multiTiAlSiN+TiN coating, where the density of normals ranges from 0.8 to 1.3 of the density corresponding to the uniform distribution (Fig. 22). The distinguished TiN deposition

plane, in most cases, is the crystallographic plane from the {111} family, or the {111} + {001} double texture occurs. This is the situation in case of specimens with the TiN+multiTiAlSiN+TiN, and $Al_2O_3$+TiN coatings, where only the {111} orientation occurs. It is also one of the two distinguished planes – apart from the {001} one – in specimens with the TiN+TiAlSiN+TiN coatings. The texture of the TiN layers in the examined material with the TiN+TiAlSiN+TiN coatings is relatively strong, and it is slightly weaker for the $Al_2O_3$+TiN. The texture is rather weak or very weak in the remaining coatings. It was found out, having conducted texture examinations of the $Al_2O_3$ corundum layers on the investigated material that all these layers have a similar structure, albeit – because of the intensity of lines and their eventual everlaying with lines of othere phases - the exact plotting of the pole figure is possible only for some of them. Therefore, analysis was limited to the texture of the $Al_2O_3$ layer of the TiN+$Al_2O_3$ coating, which is the only case when this layer occurs as the external one. This figure is presented in Figure 23. It turns out from the density of normals to the sputtered surface that the privileged crystallographic deposition plane is the {104} one. The {110} plane demonstrates the increased deposition probability too.

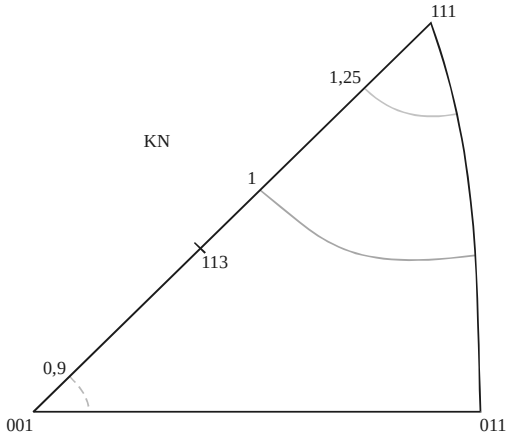


Fig. 22. Exemplary inverse for TiN layer representing the distribution of normal to the TiN+multiTiAlSiN+TiN coating surface in the (001)-(011)-(111) base triangle (KN - normal direction)

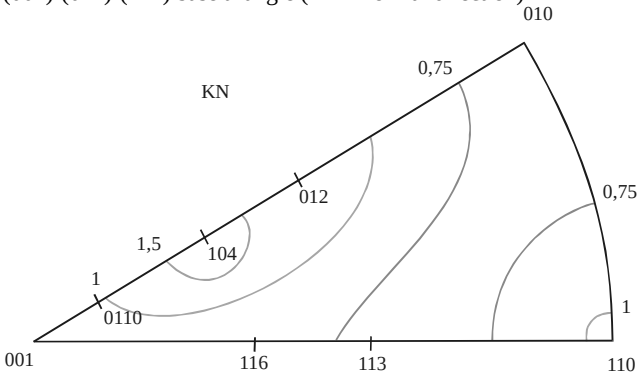


Fig. 23. Exemplary inverse for $Al_2O_3$ layer representing the distribution of normal to the TiN+$Al_2O_3$ coating surface in the (001)-(110)-(010) base triangle (KN - normal direction)

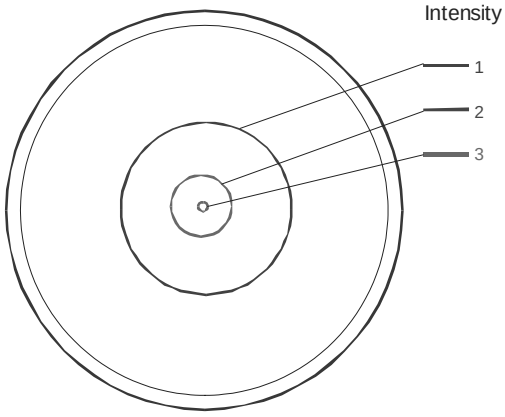


Fig 24. Polar figure {111} of the gradient TiN+(Ti,Al,Si)N+TiN coating put down onto the cermet substrate

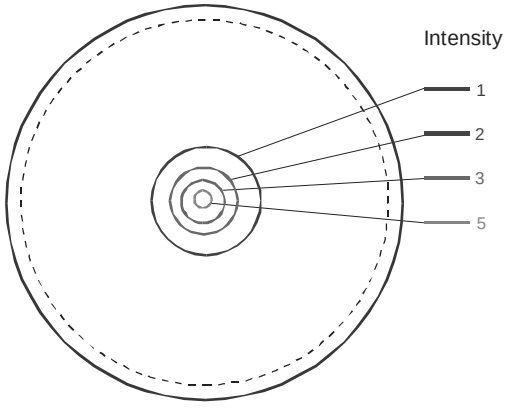


Fig 25. Polar figure {111} of the TiN+multi (Ti,Al,Si)N+TiN coating put down onto the cermet substrate

Examinations of the texture of coatings reveal their strong {111} axial texture. The lowest texturing extent (maximum value of 3, i.e., density of the {111} surfaces poles is three times bigger than in the untextured test piece) measured by the height of the maximum in the {111} figure centre is demonstrated by the TiN+(Ti,Al,Si)N +TiN coating put down onto the tool cermet (Fig. 24), and the highest texturing extent (maximum height equal to 5.5) is characteristic of the TiN+multi (Ti,Al,Si)N +TiN coating on the tool cermet substrate (Fig. 25). The coatings of the TiN + gradient or multi (Ti,Al,Si)N + TiN systems developed and investigated in this paper display the strong <111> axial texture. Crystallisation of the discussed coatings is commenced on the preferred plane with the {111} orientation, that is on the plane with the most dense arrangement of atoms, perpendicular to the plasma beam. The strong texture occurs also in case of the TiN+multi (Ti,Al,Si)N +TiN multi-layer coatings and seems to confirm also the epitaxial increase of the consecutive alternating TiN and (Ti,Al,Si)N layers, being undoubtedly favoured by the isomorphism of the pure titanium nitride and of the secondary (Ti,Al,Si)N solid solution constituting these coatings.

### 3.3. Properties of investigated materials

The microhardness tests revealed that the uncoated cemented carbides, cermets, nitride and oxide ceramics has hardness equal to 18.0 to 25.0 GPa respectively. Deposition of the PVD and CVD coatings onto the specimens causes the surface layer hardness increase reaching from 19.20 to 40.90 GPa, that is up to 100% more compared to the substrate hardness (Table 3).

The critical load values $L_c$ (AE) were determined using the scratch method with the linearly increasing load („scratch test"), characterising adherence of the investigated PVD and CVD coatings to the cermets and tool ceramics. The critical load was determined as the one corresponding to the acoustic emission increase signalling beginning of spalling of the coating. The coatings deposited onto the investigated substrates are characterised by good adherence ($L_c$ = 40-137 N), only to the TiN+(Ti,Al,Si)N+TiN gradient coating deposited onto the nitride ceramic substrate has a lower adherence equal $L_c$=22 N (Table 3).

a)

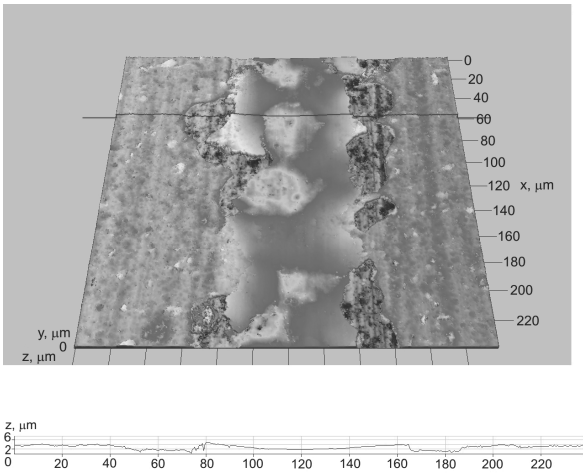


b)

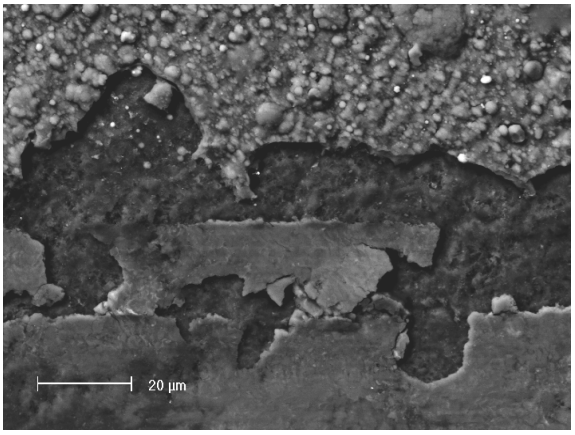


Fig. 26. Scratch test: Indenter trace of the TiN+TiAlSiN+TiN coating surface deposited onto the $Si_3N_4$ nitride ceramics substrate a) confocal microscope, b) SEM.

Defects of the PVD coatings, and especially of the three layer TiAlSiN based ones, deposited onto the nitride ceramics are characterised by a significant number of the coating spalling defects on both scratch edges and by delamination within the scratch ending up at its final part with the local coating delamination at its contact with the scratch (Fig. 26).

In the case of TiN+gradient (Ti,Al,Si)N+TiN and TiN+multi (Ti,Al,Si)N+TiN coatings deposited by the use of PVD method on $Al_2O_3$+$ZrO_2$ ceramic and cermet substrates the clear correlation between the improvement of abrasive wear resistance and wear resistance of multi-point inserts and the increase of surface layer microhardness and good adherence were stated. The very good adherence of PVD coatings to cermet substrate is a result of the fact that the source of the nitrogen for the developing coating is not only the working gas, but also nitrogen coming from the substrate alone, making diffusion mixing of elements in the interlayer easier. Therefore, not only the adhesion decides the adherence, but also the diffusion mixing of elements in the interlayer, between the substrate and the coating, with two simultaneously available sources of diffusion of elements constituting the coatings and titanium from the coating to the substrate, and also of nitrogen, and perhaps also titanium from the substrate to the coating, the more so, as the substrate temperature during the process is 550°C. However, the coatings deposited by the use of PVD methods on $Si_3N_4$ substrate do not cause the increase of cutting tool life as a result of weak substrate adherence in spite of the increase of microhardness. Undoubtedly, the influence on such significant differences in adherence of examined coatings has the fact that $Si_3N_4$ based nitride ceramic does not conduct current, which to a great degree makes the creation of PVD coatings on such substrate difficult. Clearly better adherence of CVD coatings to nitride and oxide substrates can come from the character of the same high temperature process and the fact that the substrate can be the source of the chemical element creating the layer like in the thermically activated processes. The chemical element coming from the substrate in that case nitride enables the elements to intermix diffusionally in the interlayer between the coating and the substrate. Adhesion but also diffusional intermixture of elements in the interlayer between the substrate and the coating decide about adherence.

The existence of interlayers between the $Si_3N_4$ substrate (for CVD coatings) and the $Al_2O_3$+$ZrO_2$ and cermet substrates (for PVD coatings) and between layers in the coatings causes the increase of adherence and also the improvement of cutting ability of examined materials which was confirmed among others by research carried out with the GDOES method (Fig. 27 and 28). This research confirmed presence of titanium, aluminum, silicon and oxygen as well as nitrogen in the investigated coatings and of the substrate elements, among others titanium, nickel, cobalt, zirconium, silicon, carbon, nitrogen and oxygen (Fig. 27). The analyses show that in the interlayer the increase of concentration of elements being in the composition of the substrate from the coating surface appears at the concurrent decrease of elements creating coatings. It testifies the existence of the interlayer between substrate material and the coating with earlier described diffusion migration of the chemical elements, having the influence on the improvement of adherence of deposited coatings to the substrate. However, the results cannot be interpreted unequivocally because of the heterogeneous material evaporation

Table 3
Characteristics of the investigated materials and comparison of results

| Substrate | Coating | Micro – hardness, GPa | Critical load, N (max load) | Cutting conditions | Cutting quality, $R_a$, μm | Tool life, min |
|---|---|---|---|---|---|---|
| 890 | uncoated | 18.0 | - | a = 1 mm, f = 0,10 mm/trn, V = 400 m/min, k = 70°, C45E steel | 2.4 | 1'00" |
| | TiN+TiAlSiN+TiN | 31.0 | 57.2 | | 1.9 | 20'00" |
| | TiN+multiTiAlSiN+TiN | 32.0 | 59.5 | | 1.2 | 27'00" |
| A30N | uncoated | 19.0 | - | | 2.2 | 4'00" |
| | TiN+TiAlSiN+TiN | 31.9 | 77.1 | | 1.4 | 22'00" |
| | TiN+multiTiAlSiN+TiN | 32.8 | 90.1 | | 1.2 | 33'00" |
| CM | uncoated | 24.5 | - | | 1.9 | 17'00" |
| | TiN+TiAlSiN+TiN | 33.0 | 137 (200) | | 1.5 | 55'00" |
| | TiN+multiTiAlSiN+TiN | 33.9 | 121 (200) | | 1.0 | 60'00" |
| T130A | uncoated | 25.0 | - | | 2.8 | 14'00" |
| | TiN+TiAlSiN+TiN | 33.3 | 115 (200) | | 1.5 | 43'00" |
| | TiN+multiTiAlSiN+TiN | 35.2 | 107 (200) | | 0.9 | 43'00" |
| T130Z | TiN+TiC+TiN | 30.0 | 79 (200) | | 1.5 | 35'00" |
| WidialoxG | uncoated | 18.5 | - | a = 2 mm, f = 0,15 mm/trn, V = 200 m/min, k = 70°, grey cast iron | 1.80 | 11'00" |
| | TiN+TiAlSiN+TiN | 19.2 | 40 | | 1.70 | 15'00" |
| | TiN+multiTiAlSiN+TiN | 40.9 | 76 | | 1.77 | 14'00" |
| | TiN+$Al_2O_3$ | 34.1 | 73 | | 1.87 | 17'00" |
| CC 650 | uncoated | 19.7 | - | | 2.30 | 13'30" |
| | TiN+TiAlSiN+TiN | 25.3 | 40 | | 1.63 | 17'30" |
| | TiN+multiTiAlSiN+TiN | 40.3 | 71 | | 1.37 | 19'00" |
| | TiN+$Al_2O_3$ | 34.7 | 17 | | 1.60 | 16'30" |
| CC 670 | uncoated | 18.7 | - | a = 2 mm, f = 0,2 mm/trn, V = 250 m/min, k = 70°, spheroidal cast iron | 1.53 | 8'00" |
| | TiN+TiAlSiN+TiN | 24.8 | 70 | | 1.37 | 10'30" |
| | TiN+multiTiAlSiN+TiN | 40.2 | 58 | | 1.13 | 11'00" |
| | TiN+$Al_2O_3$ | 36.7 | 18 | | 2.20 | 16'00" |
| NS260 | uncoated | 18.5 | - | a = 2 mm, f = 0,15 mm/trn, V = 200 m/min, k = 70°, grey cast iron | 5.60 | 8'00" |
| | TiN+TiAlSiN+TiN | 23.3 | 22 (100) | | 5.10 | 8'00" |
| | TiN+multiTiAlSiN+TiN | 35.2 | 23 (100) | | 4.10 | 8'00" |
| | TiN+$Al_2O_3$ | 32.5 | 83 (100) | | 2.30 | 21'30" |
| IS80 | $Al_2O_3$+TiN | 26.2 | 47 (100) | | 3.80 | 20'00" |

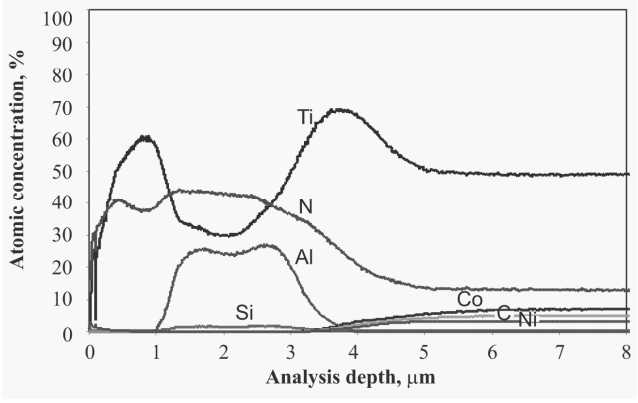


Fig. 27. Concentration changes of the TiN+ (Ti,Al,Si)N+ TiN gradient coating elements, substrate material from the T130A cermet analysed in the GDOS spectrometer

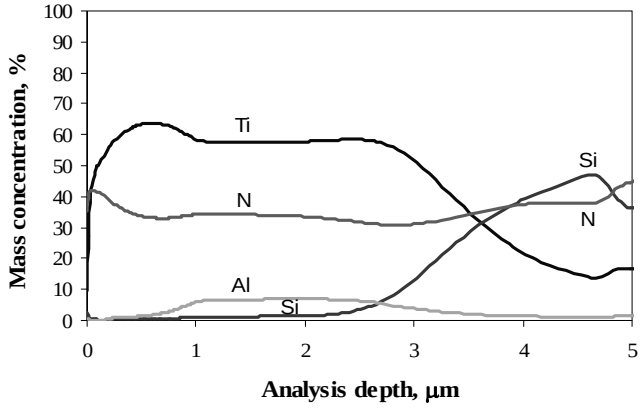


Fig. 28. Changes of concentrations of constituents of the TiN+multiTiAlSiN+TiN coating and of the substrate materials of $Si_3N_4$ ceramic nitride analysed in GDOS spectrometer

from the sample surface during the analysis. The existence of the interlayer can be explained also by the action of ions having high energy and causing the migration of elements in the interlayer, the increase of desorption of substrate surface and the appearance of defects in the substrate in the conditions of coating deposition, especially in the PVD process.

a)

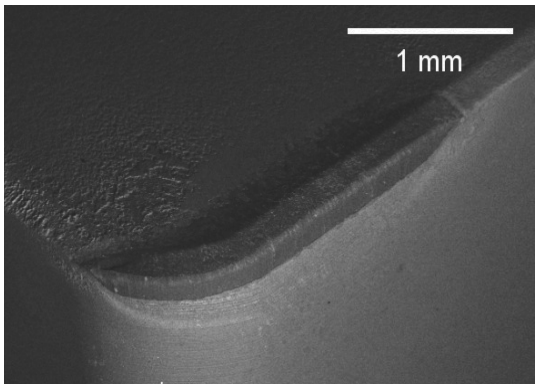


b)

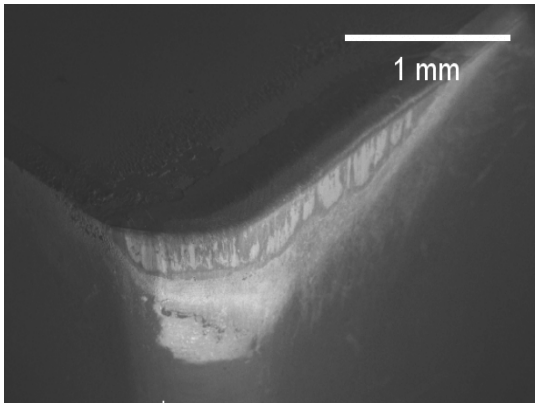


Fig. 29. Width of the VB tool flank for: a) nitride ceramics $Si_3N_4$ with deposited $TiN+Al_2O_3$ coating, b) uncoated $Si_3N_4$ nitride ceramics – after 8 minutes of machining

Examinations in the glow discharge optical emission spectrometer GDOS make it possible only to evaluate the qualitative differences of the chemical compositions in the selected micro-area of each specimen. Based on these examinations, a certain regularity was found out of the distribution of elements included in both coatings and substrate. The analysis made using the glow discharge optical emission spectrometer GDOS indicates that in the analysed cases, in the joint zone, concentration of elements included in the substrate grows from the coating surface with the simultaneous decreasing concentration of elements constituting the coatings. This may attest to the existence of the interface between the substrate material and the coating, resulting in improvement of adherence between the deposited coatings to the substrate, albeit these results cannot be interpreted unequivocally because of the inhomogeneous vaporizing of the material from the specimens' surfaces during the analysis. One may judge that the interface, both for the PVD and CVD coatings, has the diffusion character. The existence of the interface should be also connected with the increase of desorption of the substrate surface and development of defects in the substrate as well as with displacement of elements in the joint zone due to interaction of the high-energy ions (Fig. 28).

## 3.4. Cutting ability of tools reinforced with developed coatings

As a result of the research carried out it was found out that the deposition of the newly worked out multilayer and gradient nanocrystalline coatings by the use of PVD and CVD method causes the increase of cutting properties of tools made of cemented carbides, cermets, $Al_2O_3+ZrO_2$, $Al_2O_3+TiC$, $Al_2O_3+SiC_{(w)}$ oxide ceramics and $Si_3N_4$ nitride ceramics comparing to adequately uncoated tools. The increase of cutting properties indicates also tools made of $Si_3N_4$ with two-layer $TiN+Al_2O_3$ coating, analogical to tools coated by the similar system of coatings available on the market.

a)

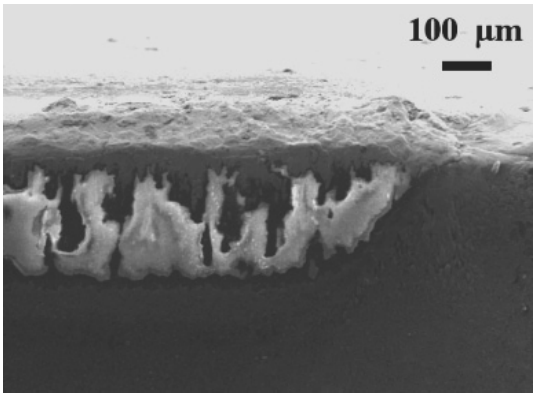


b)

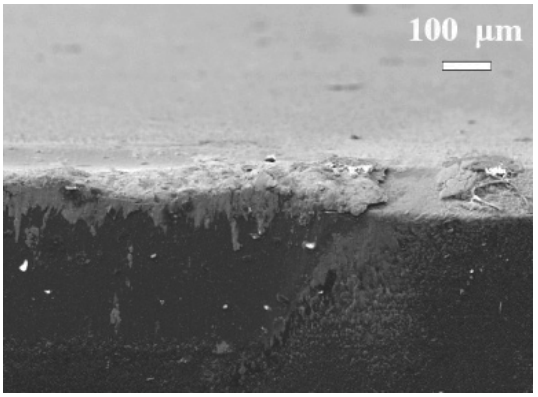


Fig. 30. Flank wear character of the: a) $Al_2O_3+ZrO_2$ ceramics with TiN+multi(Ti,Al,Si)N+TiN, b) uncoated $Al_2O_3+ZrO_2$ ceramics during the continuous cutting of the EN-GJL-250 grey cast iron

a)

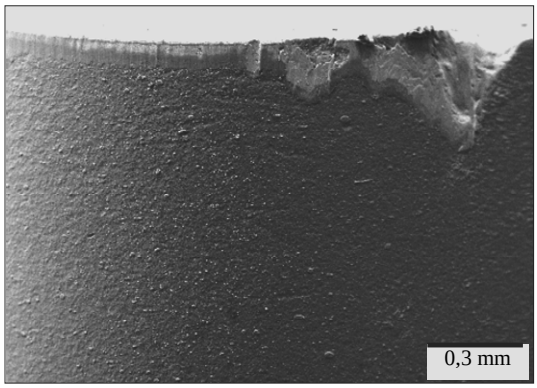


b)

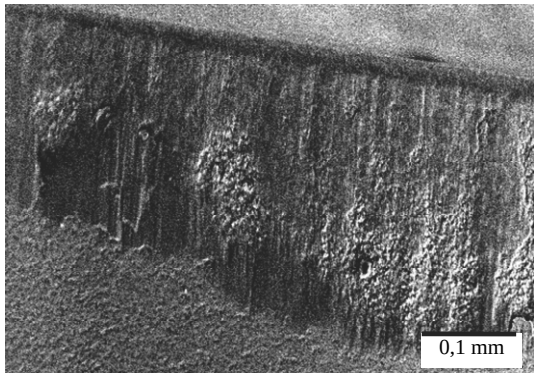


Fig. 31. Flank wear nature of the: a) T130A type cermet with the TiN+multi(Ti,Al,Si)N+TiN coating, b) uncoated T130A cermets during the continuous cutting of the C45E steel.

The detailed analysis was carried out of the relationships between the service properties of the investigated tool materials and their structure, as well as their mechanical properties, taking into account the physical phenomena occurring during the coating deposition process.

Machining tests of turning the grey cast iron with the $Si_3N_4$ ceramics revealed the clear wear resistance effect of the presence of the $Al_2O_3$+TiN and TiN+$Al_2O_3$ coatings combinations on the inserts' life. In case of inserts with the PVD coatings based on the TiN and TiAlSiN layers no tool life extension was observed, as flank failure occurs at the same time as for the uncoated insert. This is, probably, caused by a weak adhesion of these coatings to the substrate, albeit their hardness, e.g., of the TiN+multi(Ti,Al,Si)N+TiN coating, exceeds significantly hardness of other deposited coatings (Table 3). On the other hand, it was noticed that among the CVD coated inserts, the longest flank life during continuous turning corresponds to the $Si_3N_4$ with the TiN+$Al_2O_3$ coating, for which the wear band width on the tool flank reaches the value of VB=0.16 mm after 8 minutes (Fig. 29).

It was found out, based on the technological turning test of grey cast iron with the $Al_2O_3$+$ZrO_2$ ceramics, that the tool reaches the VB=0.20 mm wear criterion after t=11 min cutting time. Time of t=11 min was assumed as the comparative criterion for measurement of the wear band width for all specimens with the $Al_2O_3$+$ZrO_2$ substrate After the assumed machining test duration the smallest cutting tool flank wear band width of VB=0.11 mm was revealed in case of the TiN+$Al_2O_3$ coating (Fig. 30).

Depositing the wear resistance gradient and multi TiN+(Ti,Al,Si)N+TiN coatings on tool cermets results in increase of their wear resistance, which immediately causes, among others, increasing the tool flank life. The comparative tests of the uncoated inserts from cermets and sintered carbides carried out at the same cutting conditions indicate that the longest tool life corresponds to the CM type cermet for which the criterion flank wear band width of VB=0.2 mm was exceeded after 17 minutes of the continuous turning. The 890 type sintered carbide is characteristic if the shortest tool life, for which the criterion of the cutting edge consumption evaluation was exceeded after 1 minute of the experiment duration with the following cutting parameters: cutting speed $v_c$ = 400 m/min, feed rate f = 0.1 mm/rev, depth of cut $a_p$ = 1.0 mm. It was found out, basing on the turning test of C45E steel with the commercial T130Z cermets, that the tool reaches the VB=0.20 mm wear criterion after t=35 min cutting time (Fig. 31).

Comparison of this experimental results of the VB wear of the cemented carbides, cermets, $Al_2O_3$+$ZrO_2$, $Al_2O_3$+TiC, $Al_2O_3$+$SiC_{(w)}$ oxide ceramics and $Si_3N_4$ nitride ceramics: uncoated and coated with the PVD and CVD coatings, depending on machining time is shown in Fig. 32.

Measurements of the roughness parameter $R_a$ of the workpiece surface after machining tests reveal that the best surface quality was obtained by machining with the T130A cermet coated with the TiN+multi(Ti,Al,Si)N+TiN coating; whereas the worst quality was obtained after machining with the uncoated investigated materials.

## 4. Summary

Deposition of the gradient, multi-layer and multi-component coatings with the PVD method in the cathode arc evaporation CAE process, whose basis is the Al and Si solid secondary solution in the TiN titanium nitride, isomorphous with the alternating pure titanium nitride TiN, on tools made from oxide, nitride ceramics and tool cermets, results in the increase of mechanical properties in comparison with uncoated and coated with simple coatings tool materials, deciding thus the improvement of their working properties.

All PVD and CVD coatings deposited onto the oxide, nitride ceramics and tool cermets are characterized by a structure without pores and discontinuities and by tight adherence to themselves and of the entire multilayer coating to the substrate. Basing on the examinations of thin foils in the transmission electron microscope it was found out that the structure of the substrates and coatings is fine-grained - phase particles is smaller than 500 nm

The tool ceramics microhardness grows significantly after deposition of the PVD and CVD coatings. Most PVD and CVD coatings deposited onto the investigated substrate are characterised by good adherence. The very good adherence of PVD coatings to cermet substrate is a result of the fact that the source of the nitrogen for the developing coating is not only the working gas, but also nitrogen coming from the substrate alone, making diffusion mixing of elements in the interlayer easier.

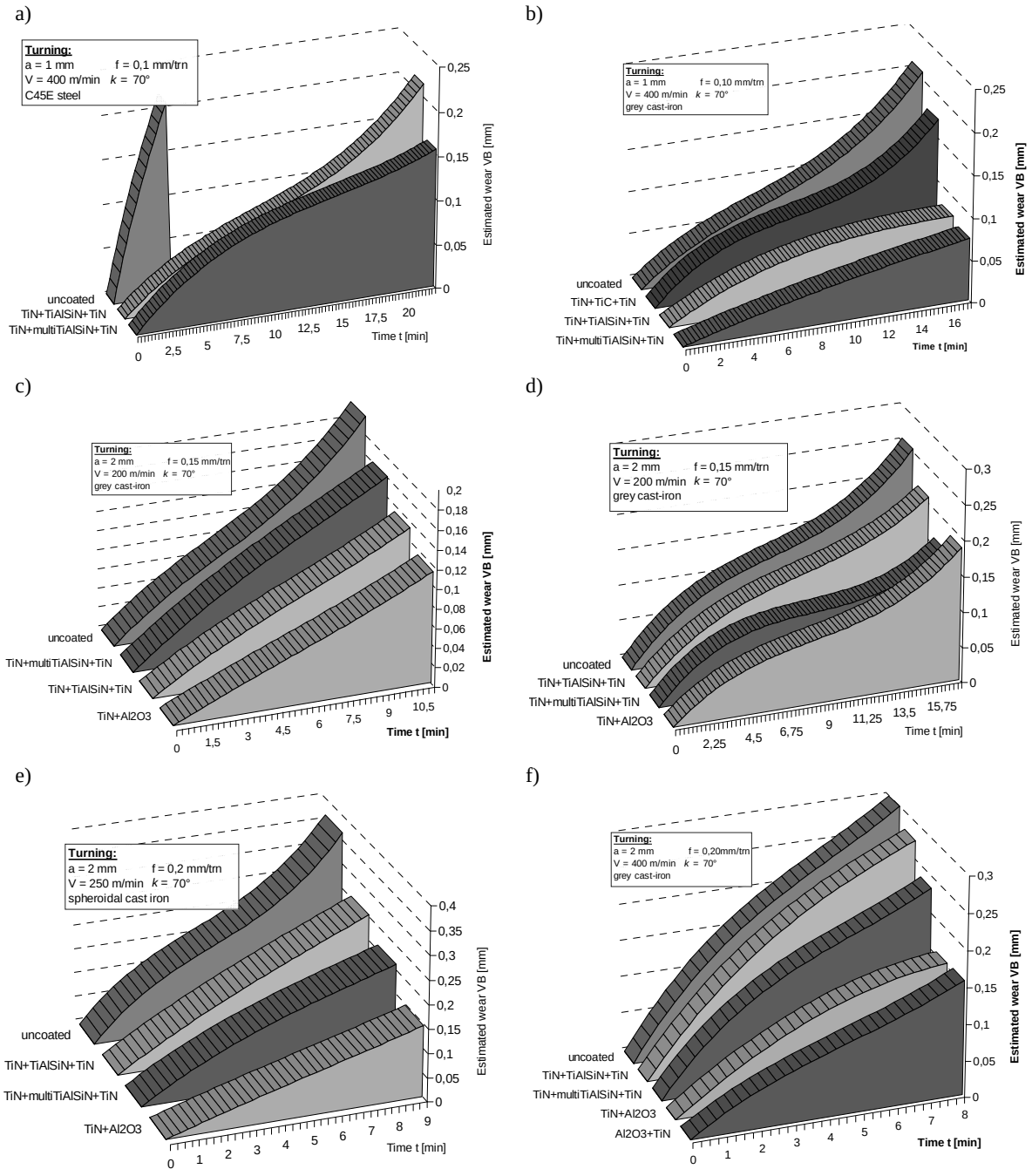


Fig. 32. Comparison of the functional properties of investigated materials: a) cemented carbides, b) cermets, c) $Al_2O_3$+$ZrO_2$, d) $Al_2O_3$+TiC, e) $Al_2O_3$+$SiC_{(w)}$ and f) $Si_3N_4$ nitride ceramics

Therefore, not only the adhesion decides the adherence, but also the diffusion mixing of elements in the interlayer, between the substrate and the coating, with two simultaneously available sources of diffusion of elements constituting the coatings and titanium from the coating to the substrate, and also of nitrogen, and perhaps also titanium from the substrate to the coating, the more so, as the substrate temperature during the process is 550°C.

However, the coatings deposited by the use of PVD methods on $Si_3N_4$ substrate have weak substrate adherence. Undoubtedly, the influence on such significant differences in adherence of examined coatings has the fact that $Si_3N_4$ based nitride ceramic does not conduct current, what to a great degree makes the creation of PVD coatings on such substrate difficult.

As a result of carried out researches it was found out that the deposition of newly worked out multilayer and gradient TiN+(Ti,Al,Si)N+TiN nanocrystalline coatings by the use of PVD method and causes the increase of cutting properties of tools made of cermets for ca. 300% and of $Al_2O_3$+$ZrO_2$ for ca. 100% comparing to adequately uncoated tools. The increase of cutting properties for ca. 100% indicates also tools made of $Si_3N_4$ with two-layer TiN+$Al_2O_3$ coating, analogical to tools coated by the similar system of coatings available on the market.

Employment of the hard wear resistant coatings deposited onto the sintered ceramic tool materials with the physical deposition from the gaseous phase (PVD) is reckoned as one of the most important achievements in the last years in the area of improvement of the service properties of ceramic cutting tools. Depositing the wear resistant coatings of the gradient and multi TiN+(Ti,Al,Si)N+TiN types onto the investigated ceramic tool materials makes it possible to achieve the clear improvement of their tool life and also of the quality of the machined surfaces, reduction of machining costs and elimination of cutting fluids used in machining. The widespread use in machining of oxide and nitride ceramics, as well as of cermets with the complex nanocrystaline coatings deposited in the PVD processes contributes to the increased interest in the contemporary "Near-Net-Shape" technology, i.e., manufacturing semi-products with the shape and dimensions as close as possible to those of the finished products.

## Acknowledgements

The research was financed partially within the framework of the research project PBZ-100/4/2004 of the Polish State Committee for Scientific Research, headed by Prof. L.A. Dobrzański.

## Notice

In the framework of the subject matter described in the given paper Prof. L.A. Dobrzański gave an inaugural lecture at the 11th International Research/Expert Conference "Trends in the Development of Machinery and Associated Technology", TMT 2007, Hammamet, Tunisia, taking place on 5-9 September, 2007.

## References

[1] L.A. Dobrzański, L.W. Żukowska, J. Mikuła, K. Gołombek, D. Pakuła, M. Pancielejko, Structure and mechanical properties of gradient PVD coatings, Journal of Materials Processing Technology 201 (2008) 310-314.
[2] K. Gołombek, J. Mikuła, D. Pakuła, L.W. Żukowska, L.A. Dobrzański, Sintered tool materials with multicomponent PVD gradient coatings, Journal of Achievements in Materials and Manufacturing Engineering 31/1 (2008) 15-22.
[3] K. Gołombek, L.A. Dobrzański, Hard and wear resistant coatings for cutting tools, Journal of Achievements in Materials and Manufacturing Engineering 24/2 (2007) 107-110.
[4] D. Pakuła, L.A. Dobrzański, Investigation of the structure and properties of PVD and CVD coatings deposited on the $Si_3N_4$ nitride ceramics Journal of Achievements in Materials and Manufacturing Engineering 24/2 (2007) 79-82.
[5] J. Mikuła, L.A. Dobrzański, PVD and CVD coating systems on oxide tool ceramics, Journal of Achievements in Materials and Manufacturing Engineering 24/2 (2007) 75-78.
[6] L.A. Dobrzański, D. Pakuła, J. Mikuła, K. Gołombek, Investigation of the structure and properties of coatings deposited on ceramic tool materials, International Journal of Surface Science and Engineering 1/1 (2007) 111-124.
[7] L.A. Dobrzański, K. Lukaszkowicz, D. Pakuła, J. Mikuła, Corrosion resistance of multilayer and gradient coatings deposited by PVD and CVD techniques, Archives of Materials Science and Engineering 28/1 (2007) 12-18.
[8] L.A. Dobrzański, J. Mikuła, K. Gołombek, Structural characteristic of the modern sintered tool materials, Materials Science Forum 530-531 (2006) 499-504.
[9] L.A. Dobrzański, D. Pakuła, Structure and properties of the wear resistant coatings obtained in the PVD and CVD processes on tool ceramics, Materials Science Forum 513 (2006) 119-133.
[10] L.A. Dobrzański, D. Pakuła, A. Kříž, M. Soković, J. Kopač, Tribological properties of the PVD and CVD coatings deposited onto the nitride tool ceramics, Journal of Materials Processing Technology 175 (2006) 179-185.
[11] L.A. Dobrzański, K. Gołombek, E. Hajduczek, Structure of the nanocrystalline coatings obtained on the CAE process on the sintered tool materials, Journal of Materials Processing Technology 175 (2006) 157-162.
[12] L.A. Dobrzański, J. Mikuła, The structure and functional properties of PVD and CVD coated $Al_2O_3$ + $ZrO_2$ oxide tool ceramics, Journal of Materials Processing Technology 167 (2005) 438-447.
[13] M. Soković, J. Mikuła, L.A. Dobrzański, J. Kopač, L. Kosec, P. Panjan , J. Madejski, A. Piech, Cutting properties of the $Al_2O_3$ + $SiC_{(w)}$ based tool ceramic reinforced with the PVD and CVD wear resistant coatings, Journal of Materials Processing Technology 164-165 (2005) 924-929.
[14] L.A. Dobrzański, D. Pakuła, Comparison of the structure and properties of the PVD and CVD coatings deposited on nitride tool ceramics, Journal of Materials Processing Technology 164-165 (2005) 832-842.
[15] L.A. Dobrzański, J. Mikuła, Structure and properties of PVD and CVD coated $Al_2O_3$ + TiC mixed oxide tool ceramics for dry on high speed cutting processes, Journal of Materials Processing Technology 164-165 (2005) 822-831.
[16] L.A. Dobrzański, K. Gołombek, Structure and properties of the cutting tools made from cemented carbides and cermets with the TiN + mono-, gradient- or multi(Ti,Al,Si)N+TiN nanocrystalline coatings, Journal of Materials Processing Technology 164-165 (2005) 805-815.
[17] D. Pakuła, L.A. Dobrzański, K. Gołombek, M. Pancielejko, A. Kříž: Structure and properties of the $Si_3N_4$ nitride ceramics with hard wear resistant coatings, Journal of Materials Processing Technology 157-158 (2004) 388-393.
[18] K. Gołombek, L.A. Dobrzański, M. Soković, Properties of the wear resistant coatings deposited on the cemented carbides substrates in the cathodic arc evaporation process, Journal of Materials Processing Technology 157-158 (2004) 341-347.

[19] L.A. Dobrzański, D. Pakuła, E. Hajduczek, Structure and properties of the multi-component TiAlSiN coatings obtained in the PVD process in the nitride tool ceramics, Journal of Materials Processing Technology 157-158 (2004) 331-340.
[20] L.A. Dobrzański, K. Gołombek, J. Kopač, M. Soković, Effect of depositing the hard surface coatings on properties of the selected cemented carbides and tool cermets, Journal of Materials Processing Technology 157-158 (2004) 304-311.
[21] M. Wysiecki, Contemporary Tool Materials, WNT, Warszawa, 1997, (in Polish).
[22] S.J. Skrzypek, New possibilities internal macro-stresses measurement using the g-sin2ψ method at the constant glancing angle (SPK), Publisher AGH, Cracow, 2002, (in Polish).
[23] Yin-Yu Chang, Da-Yung Wang, Chi-Yung Hung, Structural and mechanical properties of nanolayered TiAlN/CrN coatings synthesized by a cathodic arc deposition process, Surface and Coatings Technology 200 (2005) 1702-1708.
[24] M. Cłapa D. Batory, Improving adhesion and wear resistance of carbon coatings using Ti:C gradient layers, Journal of Achievements in Materials and Manufacturing Engineering 20 (2007) 415-418.
[25] J.A. Ghani, I.A. Choudhury, H.H. Masjuki, Wear mechanism of TiN coated carbide and uncoated cermets tools at high cutting speed applications, Journal of Materials Processing Technology 153-154 (2004) 1067-1073.
[26] W. Grzesik, Z. Zalisz, S. Król, Tribological behaviour of TiAlN coated carbides in dry sliding tests, Journal of Achievements in Materials and Manufacturing Engineering 17 (2006) 279-282.
[27] S. Hogmark, S. Jacobson, M. Larsson, Design and evaluation of tribological coatings, Wear 246 (2000) 20-33.
[28] P. Holubar, M. Jilek, M. Sima, Nanocomposite nc-TiAlSiN and nc-TiN–BN coatings: their applications on substrates made of cemented carbide and results of cutting tests, Surface and Coating Technology 120-121 (1999) 184-188.
[29] P. Holubar, M. Jilek, M. Sima, Present and possible future applications of superhard nanocomposite coatings, Surface Coatings Technology 133-134 (2000) 145-151.
[30] A. Jehn Hermann, Multicomponent and multiphase hard coatings for tribological applications, Surface and Coatings Technology 131 (2000) 433-440.
[31] I.Yu. Konyashin, Wear-resistant coatings for cermet cutting tools, Surface and Coatings Technology 71 (1995) 284-291.
[32] W. Lengauer, K. Dreyer, Functionally graded hardmetals, Journal of Alloys and Compounds 338 (2002) 194-212.
[33] T. Liu, C. Dong, S. Wu, K. Tang, J. Wang, J. Jia, TiN gradient and Ti/TiN multi-layer protective coatings on Uranium, Surface and Coating Technology 201 (2007) 6737-6741.
[34] D. Ma, S. Ma, K. Xu, Influence of Si content on nanostructured Ti–Si–N films coated by pulsed-d.c. plasma enhanced CVD, Surface and Coatings Technology 184 (2004) 182-187.
[35] R. Manaila, A. Devenyi, D. Biro, L. David, P.B. Barna, A. Kovacs, Multilayer TiAlN coatings with composition gradient, Surface and Coatings Technology 151-152 (2002) 21-25.
[36] P.H. Mayrhofer, Ch. Mitterer, L. Hultman, H. Clemens, Microstructural design of hard coatings, Progress in Materials Science 51 (2006) 1032-1114.
[37] B.A. Movchan, Functionally graded EB PVD coatings, Surface and Coatings Technology 149 (2002) 252-262.
[38] B. Navinsek, P. Panjan, I. Milosev, PVD coatings as an environmentally clean alternative to electroplating and electroless processes, Surface and Coatings Technology 116-119 (1999) 476-487.
[39] A. Noyes-William: Publishing Ceramic Cutting Tools, Edited by Whitney, E.D., 1994.
[40] S. PalDey, S.C. Deevi Cathodic arc deposited FeAl coatings: properties and oxidation characteristics, Materials Science and Engineering A355 (2003) 208-215.
[41] S. PalDey, S.C. Deevi, Properties of single layer and gradient (Ti,Al)N coatings, Materials Science and Engineering A361 (2003) 1-8.
[42] S. PalDey, S.C. Deevi, Single layer and multilayer wear resistant coatings of (Ti,Al)N: a review, Materials Science and Engineering A342 (2003) 58-79.
[43] P. Panjan, I. Boncina, J. Bevk, M. Cekada, PVD hard coatings applied for wear protection of drawing dies, Surface and Coatings Technology 200 (2005) 133-136.
[44] Z. Peng, H. Miao, W. Wang, S. Yang, Ch. Liu, L. Qi, Hard and wear-resistant titanium nitride films for ceramic cutting tools by pulsed high energy density plasma, Surface and Coatings Technology 166 (2003) 183-188.
[45] H.G. Prengel, P.C. Jindal, K.H. Wendt, A.T. Santhanam, P.L. Hegde, R.M. Penich, A new class of high performance PVD coatings for carbide cutting tools, Surface and Coatings Technology 139 (2001) 25-34.
[46] X. Qiao, Y. Hou, Y. Wu, J. Chen, Study on functionally gradient coatings of Ti-Al-N, Surface and Coating Technology 131 (2000) 462-464.
[47] S. Tjong, H. Chen, Nanocrystalline materials and coatings, Materials Science and Engineering R45 (2004) 1-88.
[48] Y.Y. Tse, D. Babonneau, A. Michel, G. Abadias: Nanometer-scale multilayer coatings combining a soft metallic phase and a hard nitride phase: study of the interface structure and morphology, Surface Coatings Technology 180-181 (2004) 470-477.
[49] T. Wierzchoń, Structure and properties of multicomponent and composite layers produced by combined surface engineering methods, Surface and Coatings Technology 180-181 (2004) 458-464.
[50] J. Zhao, J. Deng, J. Zhang, X. Ai, Failure mechanisms of a whisker-reinforced ceramic tool when machining nickel-based alloys, Wear 208 (1997) 220-225.